Charge substitution for a deep-pore residue reveals structural dynamics during BK channel gating

Xixi Chen and Richard W. Aldrich

Section of Neurobiology and Center for Learning and Memory, The University of Texas at Austin, Austin, TX 78712

The pore-lining amino acids of ion channel proteins reside on the interface between a polar (the pore) and a nonpolar environment (the rest of the protein). The structural dynamics of this region, which physically controls ionic flow, are essential components of channel gating. Using large-conductance, Ca^{2+}-dependent K^+ (BK) channels, we devised a systematic charge–substitution method to probe conformational changes in the pore region during channel gating. We identified a deep-pore residue (314 in hSlo1) as a marker of structural dynamics. We manipulated the charge states of this residue by substituting amino acids with different valence and pKa, and by adjusting intracellular pH. We found that the charged states of the 314 residues stabilized an open state of the BK channel. With models based on known structures of related channels, we postulate a dynamic rearrangement of the deep-pore region during BK channel opening/closing, which involves a change of the degree of pore exposure for 314.

The Journal of General Physiology

INTRODUCTION

Ion channel gating involves complex conformational changes in the channel protein. These conformational changes eventually converge to the pore-forming region of the channel to control ion flow across the membrane. For K^+ channels and their relatives, control of ion flow may happen via constriction of the pore at either the intracellular "bundle crossing" (Holmgren et al., 1997; Liu et al., 1997; del Camino et al., 2000; del Camino and Yellen, 2001) or the selectivity filter (Liu et al., 1996; Flynn et al., 2001; Flynn and Zagotta, 2001; Contreras and Holmgren, 2006; Contreras et al., 2008). It is believed that these two locations and their conformational changes provide the structural basis for functional processes such as activation and inactivation (Choi et al., 1991; Hoshi et al., 1991; Cuello et al., 2010a,b).

The large-conductance, Ca^{2+}-dependent K^+ (BK) channels are similar to the Kv channels in that they can be activated by membrane depolarization, but they can also be activated by increases in intracellular Ca^{2+} concentration. In that sense, they have similarities to intracellular ligand-gated ion channels such as the CNG channels. Previous work has shown that BK channel activation/deactivation does involve structural changes in the region that is equivalent to the bundle crossing in Kv channels (Li and Aldrich, 2006). But this structural change, although possibly gating the access of large intracellular blockers, does not gate the permeation of K^+ (Li and Aldrich, 2004; Wilkens and Aldrich, 2006). The activation gate in BK channels therefore seems to be located somewhere else in the pore, very likely to be at or near the selectivity filter, as in CNG channels (Contreras and Holmgren, 2006; Contreras et al., 2008). Such a notion is supported by experiments where other permeant ions, such as thallium, effect both a conformational change of the selectivity filter (Zhou and MacKinnon, 2003) and a rightward G-V shift in BK channel activation (Piskorowski and Aldrich, 2006). Here, we study further the pore conformational changes involved in BK channel gating, with the help of structural models of Kv1.2 and MthK channels.

All ion channels have a hydrophilic pore that mediates the passive flow of selected ions down their electrochemical gradients. The pore-lining parts of the channel therefore exist on the borderline between different physical environments—one that is polar (the electrolyte-filled pore) and one that is more nonpolar (the rest of the protein). To study the conformational changes of this region during gating, we developed a strategy based on the dynamic protonation range of some amino acid (such as histidine) side chains (Cymes et al., 2005; Cymes and Grosman, 2008). For example, by varying the proton concentration (pH) of the solution, the side chain of histidine can either be protonated (charged) or deprotonated (neutral). We reasoned that the charged form of the side chain should prefer the polar environment of the pore, whereas the neutral form of the side chain should have less preference for the pore.

Correspondence to Richard W. Aldrich: raldrich@mail.utexas.edu

Abbreviations used in this paper: BK, large-conductance, Ca^{2+}-dependent K^+; WT, wild type.

The Rockefeller University Press $30.00
J. Gen. Physiol. Vol. 138 No. 2 137–154
www.jgp.org/cgi/doi/10.1085/jgp.201110632

Therefore, if we mutate a certain pore-forming residue(s) into histidine and manipulate its protonation states, we could bias the side-chain orientation of those residues to turn toward or away from the pore. If, during normal gating, there are conformational changes that change the degree of pore exposure at certain locations, we should be able to uncover such structural rearrangements by observing effects on gating of protonation and deprotonation at these locations.

We scanned the pore region of hSlo1 (human BK) and indeed identified such a pore-forming residue at position 314. When the wild-type (WT) methionine was replaced by amino acids with ionizable side chains, manipulating their protonation states led to profound changes in channel gating. The effects revealed unexpected structural rearrangements of the deep-pore region during channel gating.

MATERIALS AND METHODS

Molecular biology and cell culture

Site-directed mutagenesis was conducted using Stratagene QuickChange kits (Agilent Technologies). Success of mutagenesis was confirmed by DNA sequencing (University of Texas at Austin DNA core facility). HEK293 cells (purchased from American Type Culture Collection) were cultured following standard procedures. Culture medium was high-glucose DMEM (Invitrogen) supplemented with 10% FBS (Thermo Fisher Scientific). WT and mutant BK channel cDNAs were transiently transfected into HEK cells with Lipofectamine 2000 (Invitrogen). Enhanced green fluorescent protein (Takara Bio Inc.) was cotransfected as a marker.

Electrophysiology

Recordings of BK channel currents were performed 24–48 h after transfection. Voltage-clamp recordings were performed at room temperature in the inside-out configuration on patches pulled off from HEK cells. The patch electrodes (1–3 MΩ in resistance) contained (in mM): 6 KCl, 136 KOH, 20 HEPES, and 2 $MgCl_2$, adjusted to pH 7.2 with $MeSO_3H$. Bath (intracellular side) solution contained (in mM): 6 KCl, 136 KOH, and 20 HEPES, adjusted to different pH values with $MeSO_3H$. For solutions with nominal 0 Ca^{2+}, 5 mM EDTA was included. For solutions with 200 µM Ca^{2+}, an appropriate amount of $CaCl_2$ was added to solutions with no Ca^{2+} buffer. For solutions with 1 to ∼10 µM of free Ca^{2+}, an appropriate amount of $CaCl_2$ and 5 mM EGTA were included. For solutions with 10 to ∼20 µM of free Ca^{2+}, an appropriate amount of $CaCl_2$ and 5 mM HEDTA were included. For solutions with 20 to ∼100 µM of free Ca^{2+}, an appropriate amount of $CaCl_2$ and 5 mM NTA were included. To measure free Ca^{2+} concentration, solutions with serially diluted, known Ca^{2+} concentrations (from 10 mM to 4.88 µM) were measured with Ca^{2+}-sensitive electrodes (Orion; Thermo Fisher Scientific) to generate a standard concentration–voltage curve, which was fitted with a contamination-adjusted Nernst equation and extrapolated to lower Ca^{2+} concentrations. Solutions used in the experiments were then measured with the Ca^{2+}-sensitive electrodes, and the free Ca^{2+} concentration was determined by plotting the measured voltage value on to the standard curve. K^+ concentration was manipulated to change the ionic strength of the intracellular solution. To maintain the osmotic pressure, an appropriate amount of sucrose was added. The Axopatch 200A (Axon Instruments) amplifier was used for voltage-clamp recordings. All chemicals were purchased from Sigma-Aldrich.

Data analysis

Currents were recorded from the patch and digitized using the ITC-16 A/D converter (Instrutech). Data were analogue filtered at 10 kHz, digitized at 25 kHz, collected with PULSE software (HEKA), and analyzed offline with custom software written in Igor Pro (WaveMetrics). G-V curves were obtained by tail current measurements. Similar voltage commands were used in the presence of 0 Ca^{2+} at pH 7 (or pH 5 for some mutants) to record "blank" current signals for subtracting linear leak and capacitive transients. When smaller voltage commands were used for leak traces, these traces were scaled before subtraction. Currents were normalized to the maximum current obtained in the same patch with saturating Ca^{2+} concentration at the same pH level. Group data were expressed in terms of mean ± SEM (standard error of the mean). G-V relations were fitted with a Boltzmann function [$G/G_{max} = 1/(1+e^{zF(V1/2-V)/RT})$]. Dose–response relations were fitted with a Hill equation [$y = 1/(1+(x_{1/2}/x)^n)$]. Macroscopic time-dependent kinetics was approximated by the time constant (τ_{app}) of a single-exponential fitting to the activation (at voltages with high open probability) or deactivation (at voltages with low open probability) currents. Curve fitting was performed with Igor Pro. For fitting un-normalized data, "base" and "max" terms were added to equations built in for Igor Pro.

Online supplemental material

Fig. S1 shows Ca^{2+}-dependent G-V shifts in neutral pH for WT and X314 BK channels, and current traces from the M314R BK channels are shown in Fig. S2. Figs. S1 and S2 are available at http://www.jgp.org/cgi/content/full/jgp.201110632/DC1.

RESULTS

H^+-dependent gating effects on WT BK channels (M314 (WT))

Because we were going to use protonation/deprotonation (pH changes) as one of our experimental manipulations, we first examined the effects of H^+ on WT BK channel function.

In addition to depolarization and increases in intracellular Ca^{2+} (Barrett et al., 1982; Marty and Neher, 1985; Cui et al., 1997; Cui and Aldrich, 2000; Rothberg and Magleby, 2000; Horrigan and Aldrich, 2002), an increase in intracellular proton concentration can also activate WT BK channels (Hou et al., 2008, 2009). Previous studies have localized the proton-gating effects to H365 and H394 in the RCK1 domain, with protons acting in the place of Ca^{2+} and causing a leftward shift of the steady-state G-V curve in 0 Ca^{2+} (Xia et al., 2002; Hou et al., 2008). Consistent with this idea, substituting positively charged arginines for the two protonatable RCK1 histidines (H365R:H394R) causes a similar leftward shift of the G-V curve in the absence of Ca^{2+}, as compared with WT (Hou et al., 2008). However, in the presence of saturating concentrations of Ca^{2+} (200 µM), the substituted positive charges of arginine seem to interfere with Ca^{2+} binding to the RCK1 domain. Therefore, compared with WT in 200 µM Ca^{2+}, the G-V curve for H365R:H394R in 200 µM Ca^{2+} is right-shifted (Hou et al., 2008).

In agreement with previous studies, we found that higher intracellular proton concentrations (pH 6 and

pH 5) shifted the BK WT G-V curve to the left in 0 Ca^{2+} (Figs. 1 A, 1, and 2). We also found that these higher proton concentrations, as compared with pH 7, shifted the G-V curve to the right in 200 µM Ca^{2+} (Figs. 1 A, 2, and 2), mimicking what is reported for H365R:H394R. It is therefore probable that the charges offered by the added protons work similarly to the substituted positive charges of the arginines. Consistent with this, the RCK1 double-arginine substitution largely eliminated both the H^+-induced leftward shift in 0 Ca^{2+} and the H^+-induced rightward shift in 200 µM Ca^{2+} (Fig. 1 B, 1 and 2, and Tables I and II). Interestingly, under basic pH conditions (pH 8 and pH 9), the 0 Ca^{2+} G-V curves were rightward shifted as compared with pH 7 (Fig. 1 B, 1). This would be consistent with partial neutralization of the substituted arginines in basic pH, further strengthening the idea that bound positive charges in the RCK1 domain mediate the H^+-dependent gating effects on WT BK channels. Examination of deactivation kinetics in WT BK channels revealed little pH dependence in either 0 Ca^{2+} or 200 µM Ca^{2+} (Figs. 1 C, 1 and 2, and 2). (Except for pH 5.0 with 0 Ca^{2+}, which showed slower deactivation than other pH conditions at hyperpolarized voltages of −190 to approximately −100 mV.)

Deactivation of M314H was slowed by H^+

When we mutated the methionine at 314 to histidine (M314H), the Ca^{2+}-dependent G-V relations were slightly

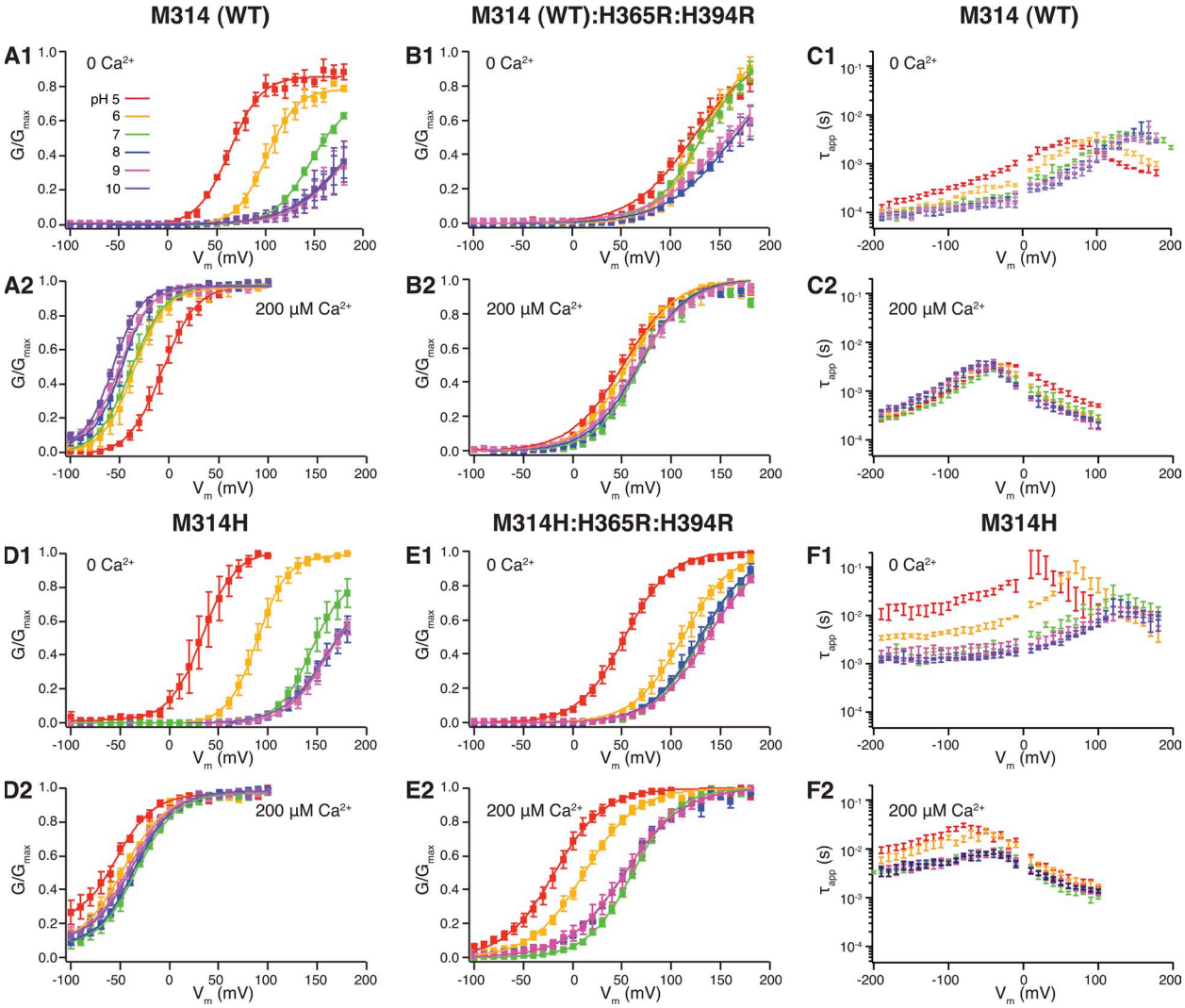

Figure 1. (A; 1) pH-dependent G-V shifts in WT BK channels in nominal 0 Ca^{2+}; (2) pH-dependent G-V shifts in WT BK channels in 200 µM Ca^{2+}; (B; 1) pH-dependent G-V shifts in M314 (WT):H365R:H394R channels in nominal 0 Ca^{2+}; (2) pH-dependent G-V shifts in M314 (WT):H365R:H394R channels in 200 µM Ca^{2+}; (C; 1)comparison of WT τ_{app}–V relations between different pH in 0 Ca^{2+}; (2) comparison of WT τ_{app}–V relations between different pH in 200 µM Ca^{2+}; (D; 1) pH-dependent G-V shifts in M314H BK channels in nominal 0 Ca^{2+}; (2) pH-dependent G-V shifts in M314H BK channels in 200 µM Ca^{2+}; (E; 1) pH-dependent G-V shifts in M314H:H365R:H394R channels in nominal 0 Ca^{2+}; (2) pH-dependent G-V shifts in M314H:H365R:H394R channels in 200 µM Ca^{2+}; (F; 1) comparison of M314H τ_{app}–V relations between different pH in 0 Ca^{2+}; (2) comparison of M314H τ_{app}–V relations between different pH in 200 µM Ca^{2+}. (See Tables I and II for fitting parameters.) Each point was calculated from a dataset with $n \geq 3$.

TABLE I

Parameter values of G-V fittings

Ca^{2+}	0										200 µM									
pH	5		6		7		8		9		5		6		7		8		9	
	$V_{1/2}$	z	$V_{1/2}$	z	$V_{1/2}$	z	$V_{1/2}$	z	$V_{1/2}$	z	$V_{1/2}$	z	$V_{1/2}$	z	$V_{1/2}$	z	$V_{1/2}$	z	$V_{1/2}$	z
WT	+63	0.7	+101	0.6	+163	1.0	+181	1.1	+168	0.9	−7	0.7	−36	0.6	−51	1.4	−48	0.6	−50	0.6
M314H	+33	0.7	+89	0.6	+151	1.2	+153	0.7	+158	0.8	−54	0.7	−47	0.9	−37	1.1	−35	0.8	−40	0.8
M314K	+83	0.8	+120	0.7	+165	1.2	+182	0.9	+161	0.8	−22	0.9	−75	0.9	−135	0.5	−80	1.2	−87	1.3
M314E	+116	1.0	+144	0.9	+178	1.2	+148	1.0	+105	1.0	+35	1.0	−15	0.8	−35	0.9				
M314D	+109	0.8	+139	1.0	+120	0.9					+28	0.8								
M314Q	+114	1.1			+205	1.1			+218	1.1	+37	1.4			−29	1.3			−29	1.3
M314N	+78	1.1			+150	1.1			+171	0.9	−88	0.7			−142	0.6			−166	0.4
MRR	+123	0.8	+132	1.1	+132	1.0	+164	0.7	+159	0.7	+51	0.9	+56	1.0	+69	1.1	+67	1.0	+66	1.0
HRR	+53	1.1	+112	1.0	131	1.0	+130	1.0	+137	0.9	−18	1.0	+12	0.9	+61	1.1	+53	0.9	+53	0.9
KRR	+135	0.6	+130	0.7	+154	0.7	+209	0.6			−41	0.6	−37	0.6	−5	0.6				
ERR	+159	0.8	+161	0.9	+153	0.8	+96	0.8	+32	0.6	+78	1.0	+78	1.0	+60	0.9	−56	0.4	−180	0.3
QRR	+153	1.0	+158	1.0	+157	1.1	+166	1.1	+178	0.9	+68	1.1	+74	1.1	+79	1.4	+80	1.0	+81	1.0
NRR	+90	0.9	+96	0.9	+97	0.9	+118	0.8	+129	0.8	−22	0.7	−9	0.7	+1	0.7	−9	0.5	−24	0.5

$V_{1/2}$ expressed in mV. Fittings were from group data with each data point having $n \geq 3$.

shifted to the left at pH 7 (Fig. S1 and Tables I and II) as compared with WT, with little change in slope. The more striking difference between M314H and WT is in deactivation kinetics (Figs. 1 F, 1 and 2, 2, and S1). At hyperpolarized voltages, the apparent deactivation time constant (τ_{app}) of M314H (1.52 ± 0.11 ms; $n = 3$) was an order of magnitude slower than that of WT (70.73 ± 8.65 µs; $n = 5$; both measured at −190 mV in 0 Ca^{2+}). There was little voltage dependence of τ_{app} at very negative voltages (−190 to approximately −100 mV) (Figs. 1 F, 1 and 2, and S1) in M314H. Elevated intracellular proton concentration prolonged channel deactivation by almost an additional order of magnitude (11.01 ± 2.75 ms and $n = 4$, at −190 mV in 0 Ca^{2+} at pH 5) (Figs. 1 F, 1, and 2).

Combining M314H with the RCK1 arginine substitutions (M314H:H365R:H394R) allowed the isolation of the effects of protonation in the pore on steady-state G-V curves

As in the WT, elevated intracellular proton concentration activated M314H (a leftward shift of the G-V curve) in 0 Ca^{2+} (Fig. 1 D, 1). However, instead of inhibiting (right-shifting the G-V curve) in 200 µM Ca^{2+} like the WT, higher proton concentration activated M314H in 200 µM Ca^{2+} (Fig. 1 D, 2, and Tables I and II). It seems that protonation of the substituted histidines at the 314 position (M314H) led to a leftward shift of the G-V curve that overcame the rightward shift via protonation of the RCK1 domain histidines in 200 µM Ca^{2+}. In 0 Ca^{2+}, however, this shift may have been masked by the H^+ effect via the RCK1 domain. When the RCK1 domain histidines were also substituted by arginines (M314H:H365R:H394R), eliminating the RCK1-mediated effects, acidic pH activated the channels (leftward G-V shifts) in both 0 and 200 µM Ca^{2+} (Fig. 1 E, 1 and 2, and Tables I and II). We conclude that the H^+ activation of M314H was a result of protonation (charging) of the substituted histidine side chains.

Alignment of the hSlo1 (human BK) sequence onto known K^+ channel structures

The H^+-mediated gating in M314H prompted us to look into the structural position of the 314 residue. Recent studies have solved the structure of the C-terminal intracellular domains of BK channels (Wu et al., 2010; Yuan et al., 2010), but the transmembrane domain structure of BK channels is still unknown. As the closest related channels with known transmembrane structures are the

TABLE II

Parameter values of G-V fittings

Ca^{2+}	0		1.3 µM		10.4 µM		85 µM		200 µM	
	$V_{1/2}$	z	$V_{1/2}$	z	$V_{1/2}$	z	$V_{1/2}$	z	$V_{1/2}$	z
WT	+163	1.0	+87	1.6	+9	1.6	−34	1.4	−51	1.4
M314H	+151	1.2	+101	1.6	+18	1.3	−31	1.3	−37	1.1
M314K	+165	1.2	+127	1.1	0	0.6	−122	0.5	−135	0.5
M314E	+178	1.2	+105	1.3	+16	1.3	−37	0.9	−35	0.9
M314D	+120	0.9	+105	1.2						

$V_{1/2}$ expressed in mV. Fittings were from group data with each data point having $n \geq 3$. All in pH 7.0.

Kv1.2 channels and the MthK channels, we threaded the protein sequence of the BK channel pore region onto the Kv1.2 and the MthK structure models. M314, highlighted in Fig. 3 A, resides in the "deep-pore" region just below the selectivity filter. This residue (a threonine in Kv1.2) was buried in the protein in the Kv1.2

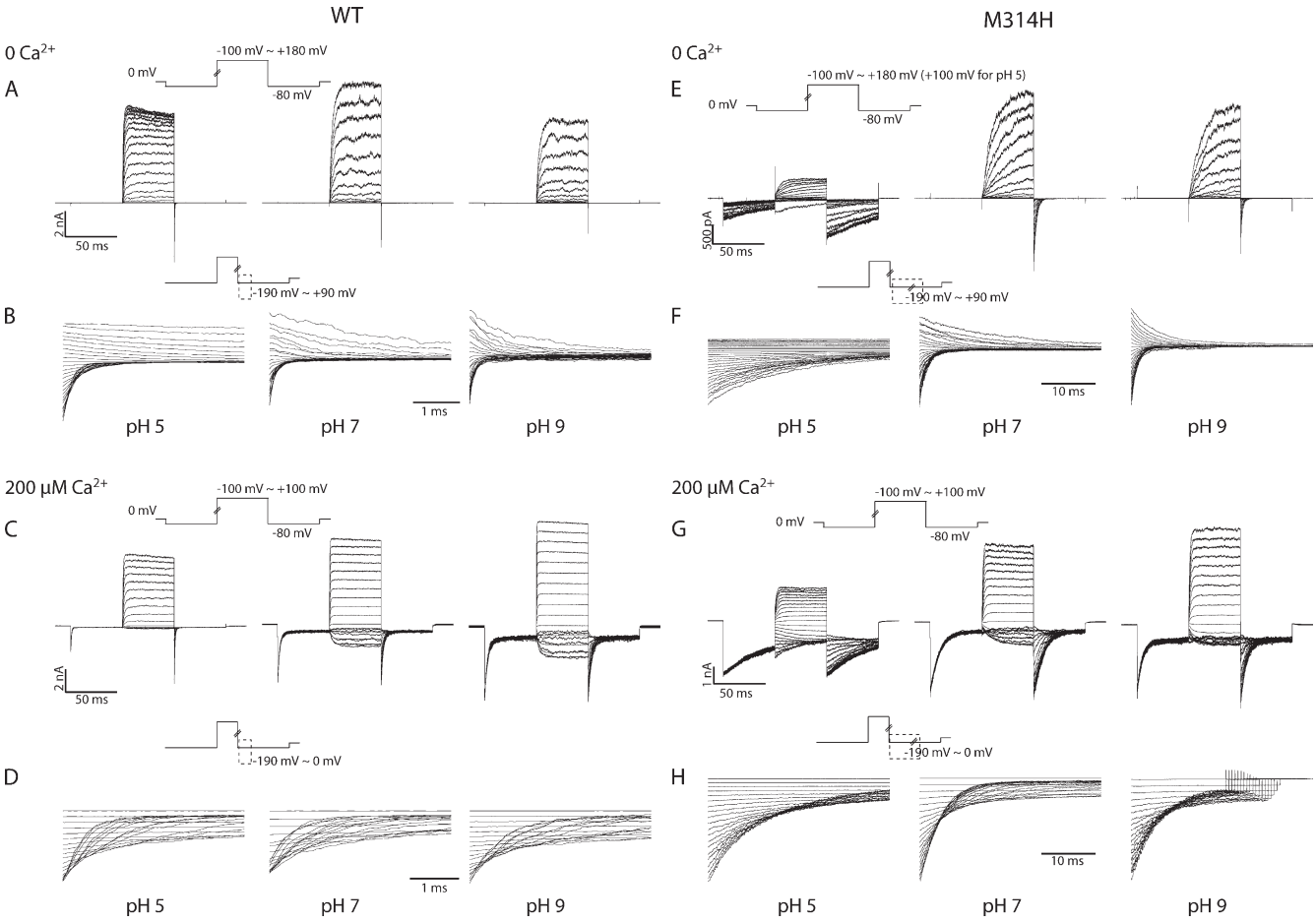

Figure 2. (A–D) Current traces in response to activation and deactivation voltage protocols for WT BK channels. (A) Current traces in response to activation voltage protocols with 0 Ca^{2+} in pH 5 (left), pH 7 (middle), and pH 9 (right). The patch was held at 0 mV, stepped down to −80 mV for 50 ms, stepped to voltages of −100 to +180 mV for 50 ms with 10-mV increments between sweeps, and then to −80 mV for 50 ms, and back to 0 mV. (B) Current traces in response to deactivation voltage protocols with 0 Ca^{2+} in pH 5 (left), pH 7 (middle), and pH 9 (right). The patch was held at 0 mV, stepped to +180 mV to activate the channels, and then down to voltage levels of −190 to +90 mV to deactivate the channels, with 10-mV increments between sweeps. Current traces of the first 3.5 ms of the deactivation period were shown (200 μs immediately after the voltage command was omitted, same for the other figures). (C) Current traces in response to activation voltage protocols with 200 μM Ca^{2+} in pH 5 (left), pH 7 (middle), and pH 9 (right). The patch was held at 0 mV, stepped down to −80 mV for 50 ms, stepped to voltages of −100 to +100 mV for 50 ms with 10-mV increments between sweeps, and then to −80 mV for 50 ms, and back to 0 mV. (D) Current traces in response to deactivation voltage protocols with 200 μM Ca^{2+} in pH 5 (left), pH 7 (middle), and pH 9 (right). The patch was held at 0 mV, stepped to +100 mV to activate the channels, and then down to voltage levels of −190 to 0 mV to deactivate the channels, with 10-mV increments between sweeps. Current traces of the first 3.5 ms of the deactivation period were shown. (E–H) Current traces in response to activation and deactivation voltage protocols for M314H BK channels. (E) Current traces in response to activation voltage protocols with 0 Ca^{2+} in pH 5 (left), pH 7 (middle), and pH 9 (right). The patch was held at 0 mV, stepped down to −80 mV for 50 ms, stepped to voltages of −100 to +180 mV for 50 ms with 10-mV increments between sweeps, and then to −80 mV for 50 ms, and back to 0 mV. (F) Current traces in response to deactivation voltage protocols with 0 Ca^{2+} in pH 5 (left), pH 7 (middle), and pH 9 (right). The patch was held at 0 mV, stepped to +180 mV to activate the channels, and then down to voltage levels of −190 to +90 mV to deactivate the channels, with 10-mV increments between sweeps. Current traces of the first 35 ms of the deactivation period were shown. (G) Current traces in response to activation voltage protocols with 200 μM Ca^{2+} in pH 5 (left), pH 7 (middle), and pH 9 (right). The patch was held at 0 mV, stepped down to −80 mV for 50 ms, stepped to voltages of −100 to +100 mV for 50 ms with 10-mV increments between sweeps, and then to −80 mV for 50 ms, and back to 0 mV. (H) Current traces in response to deactivation voltage protocols with 200 μM Ca^{2+} in pH 5 (left), pH 7 (middle), and pH 9 (right). The patch was held at 0 mV, stepped to +100 mV to activate the channels, and then down to voltage levels of −190 to 0 mV to deactivate the channels, with 10-mV increments between sweeps. Current traces of the first 35 ms of the deactivation period are shown.

structure (Fig. 3 B). In the MthK structural model, which is not as well resolved in this region, the M314 residue (a threonine in MthK) was more exposed to the pore (Fig. 3 B). Both of these structures are believed to reflect the open conformation, but they seem to differ with regard to the position of the threaded BK residue M314.

The closed-state charge interaction hypothesis versus the open-state charge stabilization hypothesis

Because the Kv1.2 structure is better resolved in the deep-pore region, and because Kv1.2 is a eukaryotic channel like BK (hSlo1), we first assumed that the Kv1.2-based structure model was a reasonable approximation of the open conformation in BK channels. If the Kv1.2 structure approximates the BK open state, the substituted H314 residues would also be buried when the channel is open. Upon protonation, the substituted histidine side chains should prefer a polar environment and become more exposed to the pore. Based on the homology model and the H^+ activation of M314H and M314H:H365R:H394R, we hypothesized that the H314-exposed conformation corresponded to a closed BK channel (Fig. 3 C, 1), and that the charges at this position from the four subunits were close enough in the pore that they electrostatically repelled each other, making the closed conformation energetically unfavorable, leading to the observed leftward shift of G-V curves.

However, a destabilized closed state does not readily explain the drastic slowing of macroscopic current kinetics (τ_{app}), especially at very negative voltages (deactivation at −190 mV, for example). Generally speaking, at high voltages, this τ_{app} value is mainly determined by the rate constant of the channel going from closed to open states (α). At very negative voltages, this τ_{app} value is dominated

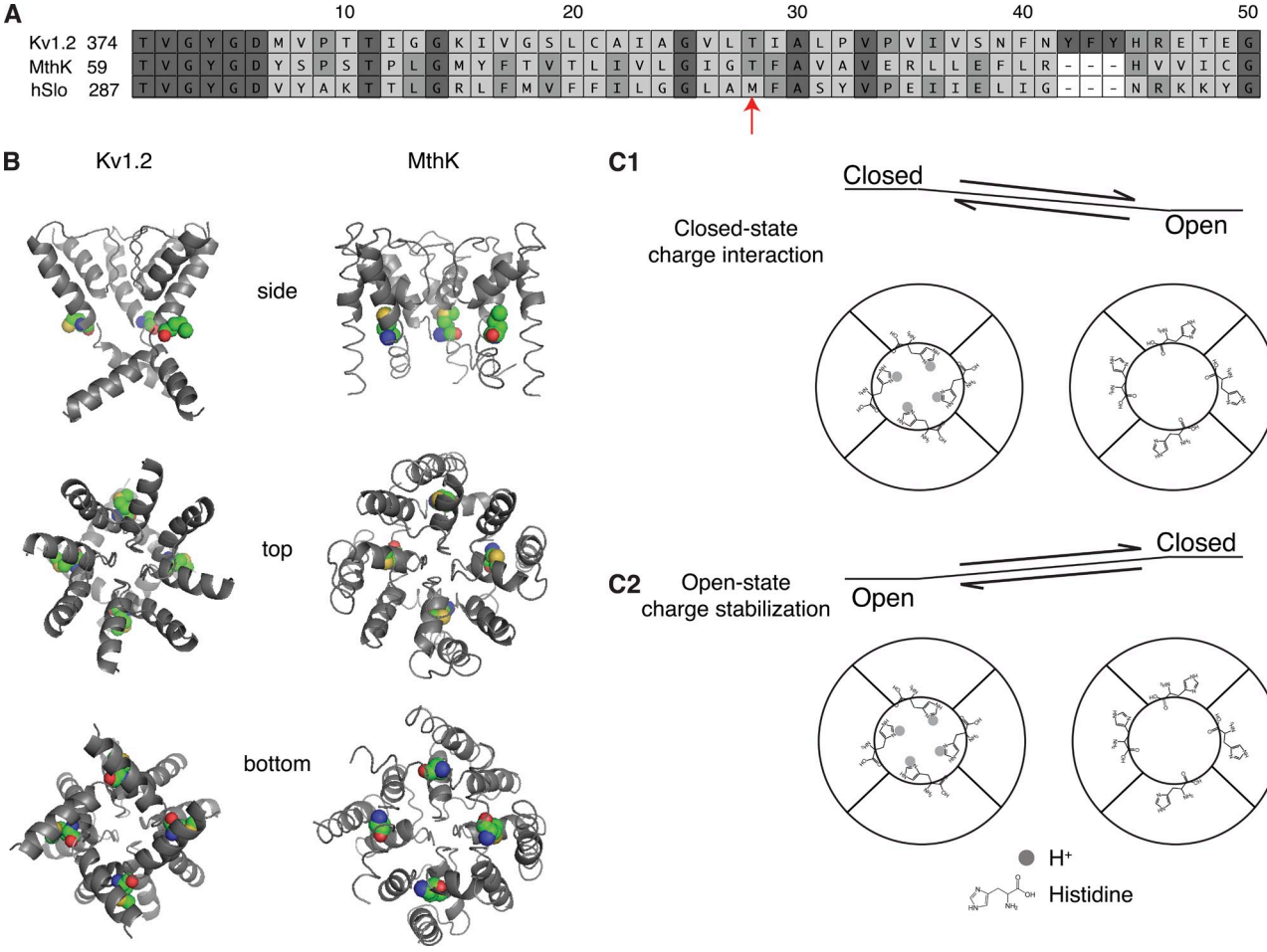

Figure 3. (A) Amino acid sequence alignment of Kv1.2, MthK, and hSlo1 (human BK) in the pore region. Alignment started from the T of the TVGYGD signature sequence of the selectivity filter. (B) PyMol-generated structure models of the BK channel pore region based on the Kv1.2 or the MthK structure. Equivalent BK amino acid residues were substituted into the Kv1.2 or MthK sequence. One of the four subunits was removed in the side view to reveal the pore. Top view is from the extracellular side of the channel. Bottom view is from the intracellular side of the channel. The M314 position in BK is highlighted in colors: green, C; blue, N; red, O; gold, S. (C; 1) Diagram of the closed-state charge interaction hypothesis, with the middle of the concentric circles representing the pore of the channel. Each one of the subunits had a substituted histidine. (2) Diagram of the open-state charge stabilization hypothesis.

by the rate constant of the channel going from open to closed states (β). A destabilized closed state would indicate a fast α, but our kinetic data are suggesting a slow β.

To account for both the slow deactivation and the leftward shift of G-V curves induced by protonation of M314H, we considered an alternative hypothesis that proposes an energetically favorable open state. According to this hypothesis, the 314 side-chain–exposed conformation would correspond to an open BK channel (Fig. 3 C, 2), and the charges at this position (for example, the protonated histidines in M314H), by preferring the polar environment of the pore, stabilize the channel in the open conformation, leading to the observed effects of leftward G-V shifts and slow deactivation.

Both the "closed state charge interaction" and the "open state charge stabilization" hypotheses could explain the H^+-induced steady-state G-V shifts in M314H, but the "open-state" hypothesis is better at accounting for the H^+-induced slowing of deactivation in M314H. On the other hand, the "closed-state" hypothesis is in better agreement with the Kv1.2-based structural model for an open channel.

As both hypotheses share the same central argument for protons mediating a charge effect on gating energetics, we further evaluated this argument with more charge substitutions at the 314 position. We were interested in how the amount of charge at 314 would correlate with the extent of G-V shifts and/or changes in deactivation kinetics, and whether negative charges would have similar effects as positive charges. With analyses of the G-V shifts, we looked at both the M314X and the M314X:H365R:H394R mutants whenever we saw significant contribution of the RCK1 mechanism to the H^+-induced G-V shifts. However, because H^+ did not cause significant changes in the deactivation kinetics of WT BK channels (Fig. 1 C, 1 and 2, at −190 mV), we limited our analyses of H^+-induced changes in deactivation τ_{app} to the M314X mutants to avoid possible complications introduced by the substituted RCK1 arginines.

Deactivation of M314K was slow in neutral pH

When we substituted lysine (K) into the 314 position, we saw that deactivation was slower for M314K than M314H, at pH 7 (Figs. 4 C, 1 and 2, 5, B and D, and S1). As a matter of fact, the deactivation kinetics of M314K in pH 7 (6.48 ± 1.26 ms and $n = 4$, at −190 mV in 0 Ca^{2+}; 8.76 ± 1.90 ms and $n = 3$, at −190 mV in 200 μM Ca^{2+}) were similar to those of M314H in pH 5. This is consistent with the pKa difference between the two amino acids, with lysine having a higher pKa (10.8 in water) than histidine (6.0 in water). Similar to what we observed with M314H, acidic conditions (pH 6 and pH 5) further slowed deactivation (as compared with pH 7) for M314K (Fig. 4 C, 1 and 2), consistent with protonation of the lysine side chains at more acidic pH.

H^+-dependent shift of G-V curves for M314K and M314K:H365R:H394R

For M314K, higher proton concentrations shifted the G-V curves to the left in 0 Ca^{2+} and to the right in 200 μM Ca^{2+} (Fig. 4 A, 1 and 2, and Tables I and II). Protons, like in the M314H mutant, were likely to act via at least two routes to affect BK channel gating. One is through charging of the 314 side chain; the other is through charging the RCK1 histidines (H365 and H394). As with M314H when we added the arginine substitution for the RCK1 histidines to the lysine substitution at 314 (M314K:H365R:H394R), we found that in both 0 and 200 μM Ca^{2+}, the G-V curves were shifted to the left in lower pH and to the right in higher pH, as compared with pH 7 (Fig. 4 B, 1 and 2, and Tables I and II).

Deactivation of M314E faithfully followed changes in intracellular H^+ concentrations

To test whether negative charges have the same effects as positive charges, we substituted glutamic acid into the M314 position. At pH 7, the M314E channels behaved much like WT BK channels (Figs. 1, WT, pH 7; 4, M314E, pH 7; S1; and 5). There was little difference in Ca^{2+}-dependent G-V relations between M314E and WT. Deactivation was slower than WT at very negative voltages (0.56 ± 0.06 ms and $n = 4$, at −190 mV in 0 Ca^{2+}; 1.72 ± 0.004 ms and $n = 3$, at −190 mV in 200 μM Ca^{2+}) (Fig. S1), but the difference was much smaller than what we saw with M314H and M314K.

However, M314E behaved like WT only at pH 7. Deactivation of M314E in 0 Ca^{2+} was progressively slower with decreasing $[H^+]$ (increasing pH) (Figs. 4 F, 1, and 5 F), which is the opposite direction from the cases for M314H and M314K, as both deactivate more slowly with increased protonation. In 200 μM Ca^{2+}, these channels were open even at very negative voltages in basic pH (Figs. 4 D, 2, and 5 G), whereas acidic pH made the deactivation faster (Figs. 4 F, 2, and 5 H).

The glutamate residues were likely to be charged under basic conditions, whereas the histidine and lysine residues were likely to be charged under acidic conditions. For these three mutants, it appears that charging the substituted side chains led to slow deactivation, and that neutralizing the substituted side chains made the deactivation faster.

H^+-dependent shift of G-V curves for M314E and M314E:H365R:H394R

In 0 Ca^{2+}, elevated proton concentration (pH 6 and pH 5) negatively shifted the G-V curve of M314E as compared with pH 7. Interestingly, reduced proton concentration (pH 8, pH 9, and pH 10) also shifted the G-V curve to more negative voltages (Fig. 4 D, 1, and Tables I and II). The G-V shift from pH 7 was almost the same between pH 5 and pH 9, although the deactivation kinetics were dramatically different between these two conditions

(see above). We reasoned that the leftward G-V shift by acidic pHs was probably a result of the RCK1 histidines, whereas the leftward G-V shift by basic pHs was likely a charging effect of the substituted glutamate at 314.

With 200 µM Ca^{2+}, acidic pH shifted the M314E G-V curves to the right, and basic pHs shifted those curves to the left (Fig. 4 D, 2, and Tables I and II). Again, it seems that the rightward shift in acidic pH follows the same mechanisms in WT, as protons interfere with Ca^{2+} binding in the RCK1 domain. Basic pHs, by charging the substituted glutamate at 314, and not interfering with Ca^{2+} binding in RCK1, shifted the G-V curves to the left.

In the triple mutant M314E:H365R:H394R, where the RCK1 histidine–mediated proton effects should be eliminated, we saw little G-V shift by acidic pHs, as compared with pH 7, in 0 Ca^{2+}, and a small rightward shift in 200 µM Ca^{2+}. Basic pHs still caused leftward G-V shifts (Fig. 4 E, 1 and 2). That is, charging the glutamate at 314 (in basic pHs) shifted the G-V curves to the left; neutralizing the glutamate at 314 (in acidic pHs) led to either no shift or rightward shift of the G-V curves.

Comparing the isolated (from the RCK1 histidine–mediated mechanism) effects of M314 histidine, lysine, and glutamic acid substitutions, the direction of the G-V shifts seemed to follow a single mechanism. Conditions that favor the charged forms of the side chains at the 314 position (low pHs for histidine and lysine, high pHs for glutamate) led to leftward shifts of the G-V curves

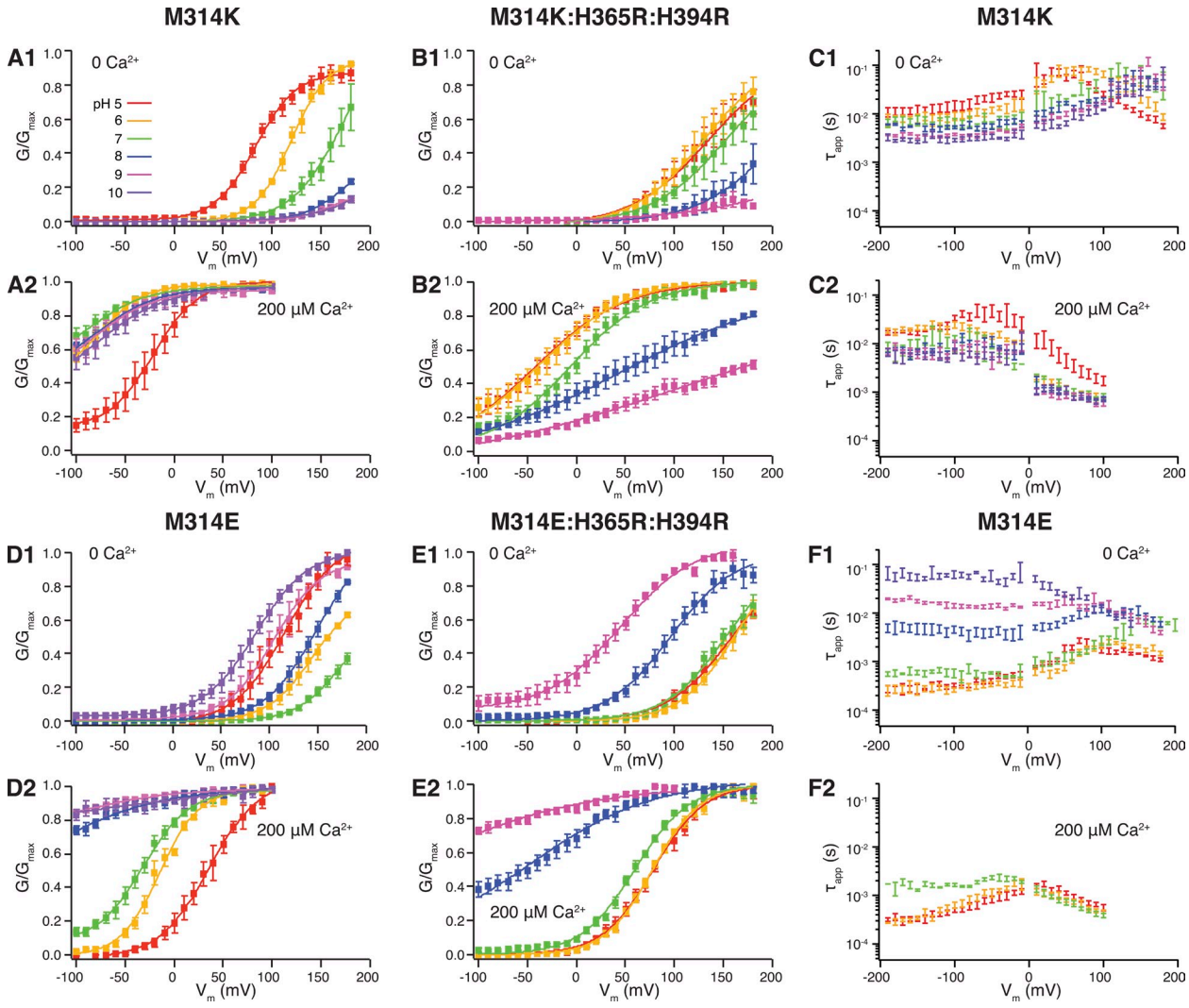

Figure 4. (A; 1) pH-dependent G-V shifts in M314K BK channels in nominal 0 Ca^{2+}; (2) pH-dependent G-V shifts in M314K BK channels in 200 µM Ca^{2+}; (B; 1) pH-dependent G-V shifts in M314K:H365R:H394R channels in nominal 0 Ca^{2+}; (2) pH-dependent G-V shifts in M314K:H365R:H394R channels in 200 µM Ca^{2+}; (C; 1) comparison of M314K τ_{app}–V relations between different pH in 0 Ca^{2+}; (2) comparison of M314K τ_{app}–V relations between different pH in 200 µM Ca^{2+}; (D; 1) pH-dependent G-V shifts in M314E BK channels in nominal 0 Ca^{2+}; (2) pH-dependent G-V shifts in M314E BK channels in 200 µM Ca^{2+}; (E; 1) pH-dependent G-V shifts in M314E:H365R:H394R channels in nominal 0 Ca^{2+}; (2) pH-dependent G-V shifts in M314E:H365R:H394R channels in 200 µM Ca^{2+}; (F; 1) comparison of M314E τ_{app}–V relations between different pH in 0 Ca^{2+}; (2) comparison of M314E τ_{app}–V relations between different pH in 200 µM Ca^{2+}. (See Tables I and II for fitting parameters.) Each point was calculated from a dataset with $n \geq 3$.

and slower deactivation. Conditions that favor the neutralized forms of the side chains at the 314 position (high pHs for histidine and lysine, low pHs for glutamate) led to either no shift or a rightward shift of the G-V curves.

M314D was constitutively open

When the other negatively charged amino acid (aspartic acid) was substituted into the M314 position, the channels were constitutively open. That is, in pH 7,

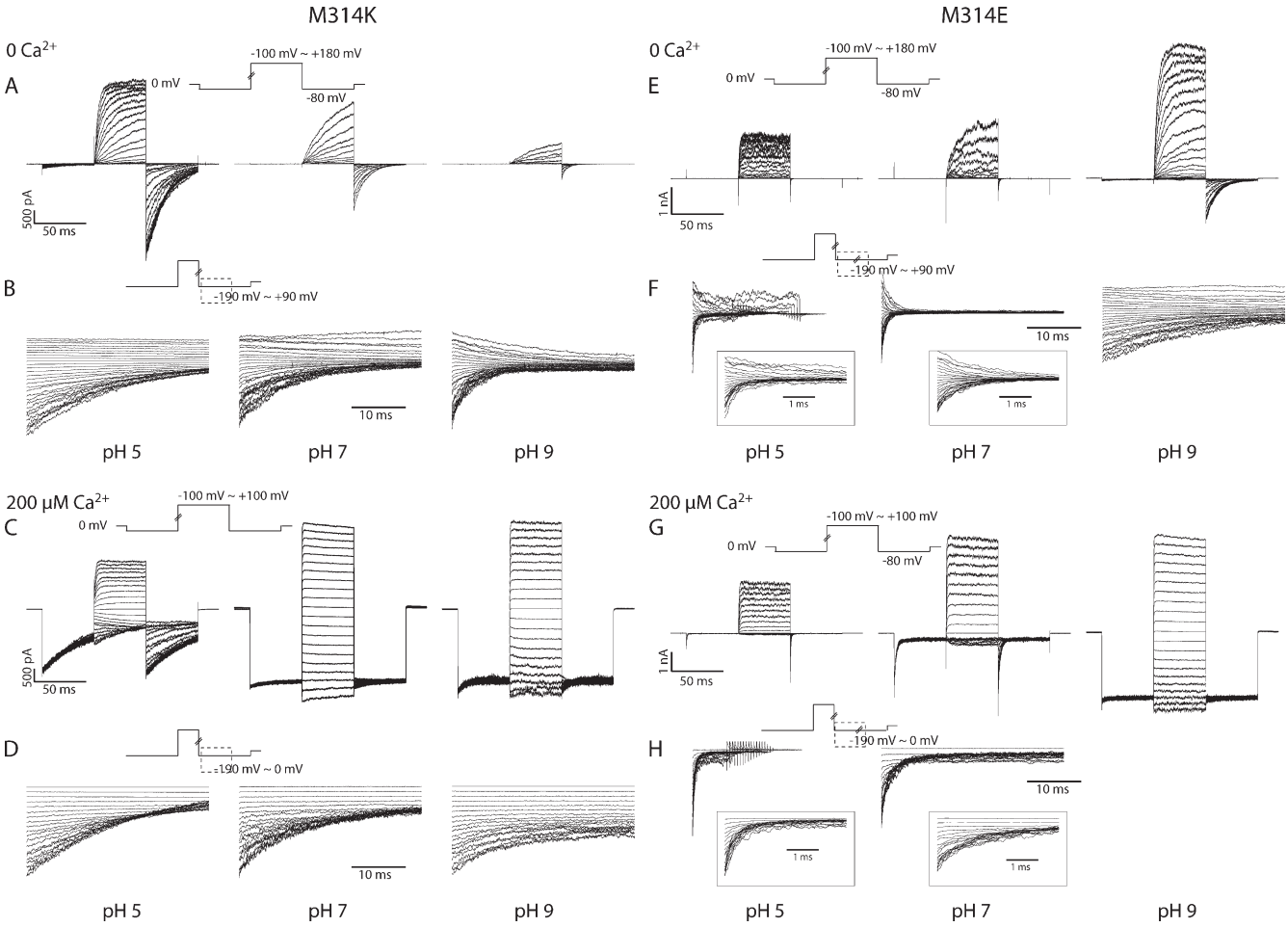

Figure 5. (A–D) Current traces in response to activation and deactivation voltage protocols for M314K BK channels. (A) Current traces in response to activation voltage protocols with 0 Ca^{2+} in pH 5 (left), pH 7 (middle), and pH 9 (right). The patch was held at 0 mV, stepped down to −80 mV for 50 ms, stepped to voltages of −100 to +180 mV for 50 ms with 10-mV increments between sweeps, and then to −80 mV for 50 ms, and back to 0 mV. (B) Current traces in response to deactivation voltage protocols with 0 Ca^{2+} in pH 5 (left), pH 7 (middle), and pH 9 (right). The patch was held at 0 mV, stepped to +180 mV to activate the channels, and then down to voltage levels of −190 to +90 mV to deactivate the channels, with 10-mV increments between sweeps. Current traces of the first 35 ms of the deactivation period are shown. (C) Current traces in response to activation voltage protocols with 200 µM Ca^{2+} in pH 5 (left), pH 7 (middle), and pH 9 (right). The patch was held at 0 mV, stepped down to −80 mV for 50 ms, stepped to voltages of −100 to +100 mV for 50 ms with 10-mV increments between sweeps, and then to −80 mV for 50 ms, and back to 0 mV. (D) Current traces in response to deactivation voltage protocols with 200 µM Ca^{2+} in pH 5 (left), pH 7 (middle), and pH 9 (right). The patch was held at 0 mV, stepped to +100 mV to activate the channels, and then down to voltage levels of −190 to 0 mV to deactivate the channels, with 10-mV increments between sweeps. Current traces of the first 35 ms of the deactivation period are shown. (E–H) Current traces in response to activation and deactivation voltage protocols for M314E BK channels. (E) Current traces in response to activation voltage protocols with 0 Ca^{2+} in pH 5 (left), pH 7 (middle), and pH 9 (right). The patch was held at 0 mV, stepped down to −80 mV for 50 ms, stepped to voltages of −100 to +180 mV for 50 ms with 10-mV increments between sweeps, and then to −80 mV for 50 ms, and back to 0 mV. (F) Current traces in response to deactivation voltage protocols with 0 Ca^{2+} in pH 5 (left), pH 7 (middle), and pH 9 (right). The patch was held at 0 mV, stepped to +180 mV to activate the channels, and then down to voltage levels of −190 to +90 mV to deactivate the channels, with 10-mV increments between sweeps. Current traces of the first 35 ms of the deactivation period are shown. Traces in the insets show the first 3.5 ms of deactivation. (G) Current traces in response to activation voltage protocols with 200 µM Ca^{2+} in pH 5 (left), pH 7 (middle), and pH 9 (right). The patch was held at 0 mV, stepped down to −80 mV for 50 ms, stepped to voltages of −100 to +100 mV for 50 ms with 10-mV increments between sweeps, and then to −80 mV for 50 ms, and back to 0 mV. (H) Current traces in response to deactivation voltage protocols with 200 µM Ca^{2+} in pH 5 (left), pH 7 (middle), and pH 9 (right). The patch was held at 0 mV, stepped to +100 mV to activate the channels, and then down to voltage levels of −190 to 0 mV to deactivate the channels, with 10-mV increments between sweeps. Current traces of the first 35 ms of the deactivation period are shown. Traces in the insets show the first 3.5 ms of deactivation.

M314D channels had appreciable open probability even with no Ca^{2+} and large hyperpolarization (Figs. 6 and S1). Ca^{2+}, depolarization, or deprotonation each led to further channel activation (Fig. 6). Among all the tested conditions, M314D channels can only close in pH 5 (the lowest pH level attempted) (Fig. 6).

As in the other single 314 mutants, there are probably two separate, proton-mediated mechanisms in M314D. One is the hydrolyzing condition of the substituted aspartate, which pH 5 should bias toward neutralizing. The other is the hydrolyzing condition of the RCK1 histidines, which pH 5 should bias toward charging. In 0 Ca^{2+}, pH 5 should cause a leftward G-V shift via RCK1 and a rightward shift via 314D. It seems that the balance of the two mechanisms eventually led to a rightward shift, with the 314D mechanism dominating. In 200 µM Ca^{2+}, both of these mechanisms should lead to a rightward G-V shift in pH 5, as seen.

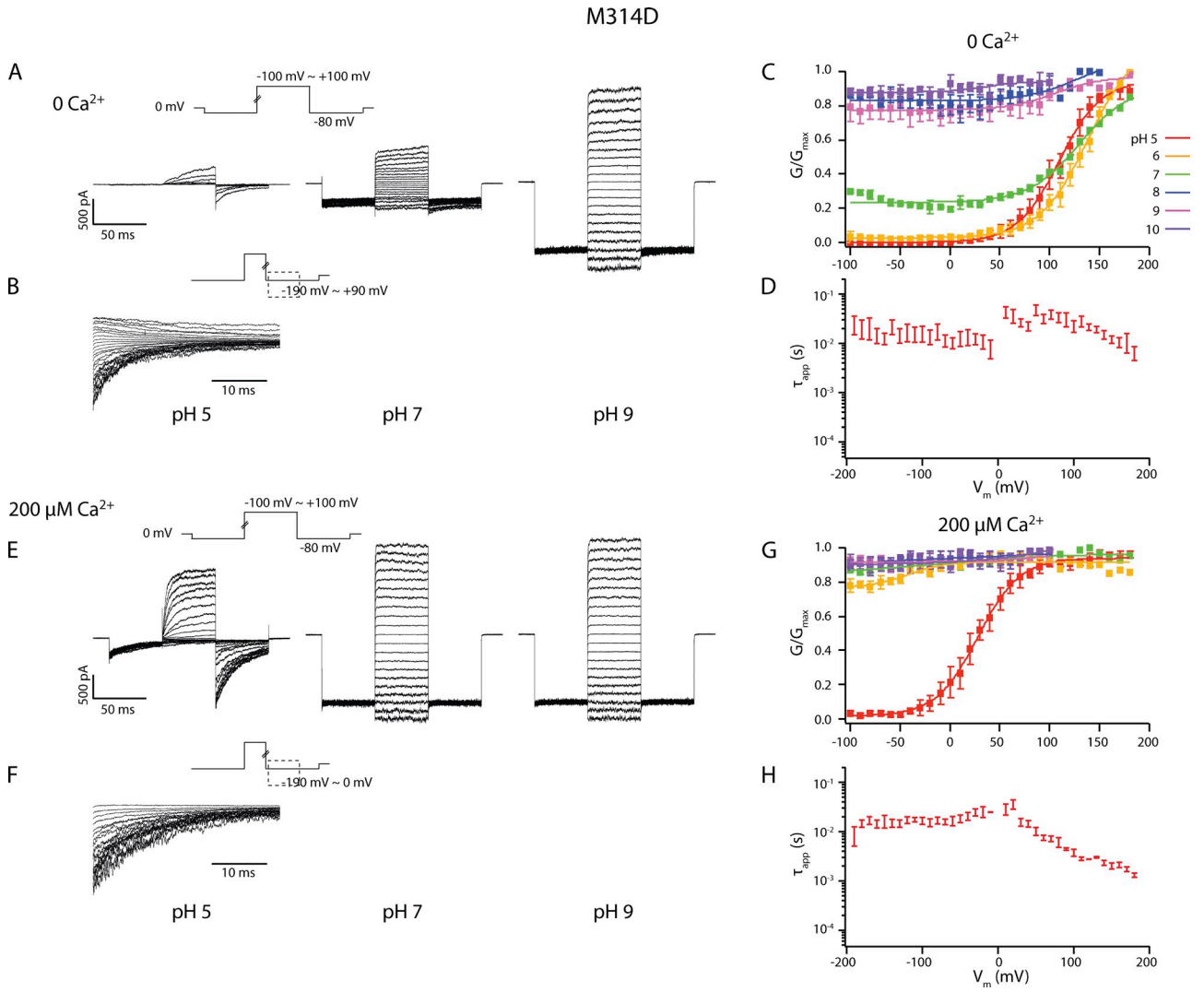

Figure 6. (A) Current traces in response to activation voltage protocols for M314D in 0 Ca^{2+} in pH 5, pH 7, and pH 9. The patch was held at 0 mV, stepped down to −80 mV for 50 ms, stepped to voltages of −100 to +100 mV for 50 ms with 10-mV increments between sweeps, and then to −80 mV for 50 ms, and back to 0 mV. (B) Current traces in response to deactivation voltage protocols for M314D in 0 Ca^{2+} in pH 5. The patch was held at 0 mV, stepped to +100 mV to activate the channels, and then down to voltage levels of −190 to +90 mV to deactivate the channels, with 10-mV increments between sweeps. Current traces of the first 35 ms of the deactivation period are shown. (C) pH-dependent G-V shifts in M314D BK channels in nominal 0 Ca^{2+}. (D) τ_{app}–V relations of M314D in pH 5 and 0 Ca^{2+}. (E) Current traces in response to activation voltage protocols for M314D in 200 µM Ca^{2+} in pH 5, pH 7, and pH 9. The patch was held at 0 mV, stepped down to −80 mV for 50 ms, stepped to voltages of −100 to +100 mV for 50 ms with 10-mV increments between sweeps, and then to −80 mV for 50 ms, and back to 0 mV. (F) Current traces in response to deactivation voltage protocols for M314D in 200 µM Ca^{2+} and pH 5. The patch was held at 0 mV, stepped to +100 mV to activate the channels, and then down to voltage levels of −190 to 0 mV to deactivate the channels, with 10-mV increments between sweeps. Current traces of the first 35 ms of the deactivation period are shown. (G) pH-dependent G-V shifts in M314D BK channels in 200 µM Ca^{2+}. (H) τ_{app}–V relations of M314D in pH 5 and 200 µM Ca^{2+}. Each point was calculated from a dataset with $n \geq 3$.

At 0 Ca^{2+} and low voltages, M314D effectively became a proton-gated channel that is open at neutral and basic pH but can be closed with intracellular protons. We plotted the open probability of M314D at −100 mV in 0 Ca^{2+} against intracellular pH (Fig. 7). We found the pKa of this effect to be 7.23, which is significantly higher than the pKa of aspartate in water (∼4.0), suggesting an environment in the pore significantly different from bulk solution.

Lack of position 314–mediated, H^+-dependent gating with nonprotonatable polar side chains

To further confirm that the H^+-dependent gating effects we saw in the 314 mutants were indeed mediated by the charges of the substituted side chains, we next made the M314Q and M314N mutants. Glutamine (Q) is essentially the same as glutamic acid (E), except for the nonionizable side chain. Asparagine (N) is the nonionizable analogue of aspartic acid (D).

For M314Q, in 0 Ca^{2+}, there was little shift of G-V curves between pH 9 and pH 7, whereas pH 5 shifted the G-V curve to the left (Fig. 8 A, 1). In 200 µM Ca^{2+}, again there was virtually no G-V shift between pH 9 and pH 7, but pH 5 shifted the G-V curve to the right (Fig. 8 A, 2). Comparing these observations to M314E, the 314E-mediated, deprotonation-dependent leftward G-V shift was absent from M314Q. The acidic pH–induced G-V shift was intact, which should be through the RCK1 histidine mechanism.

When we tested the M314Q:H365R:H394R mutant, in both 0 Ca^{2+} and 200 µM Ca^{2+}, the G-V curves in all pH conditions were very similar to each other (Fig. 8 B, 1 and 2, and Tables I and II), and are similar to those for M314 (WT):H365R:H394R (Tables I and II). Deactivation kinetics were not significantly dependent on pH either (Fig. 9 B, 1 and 2). Therefore, substituting glutamine (Q) into the 314 location did not lead to the position 314–mediated, H^+-dependent gating effects we saw for M314E.

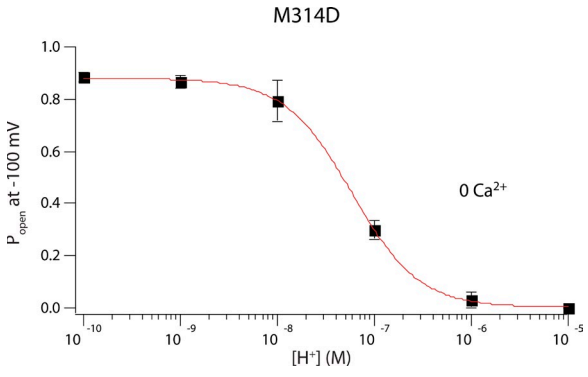

Figure 7. For M314D, open probability of the channels at −100 mV in 0 Ca^{2+} was plotted against approximate intracellular H^+ concentration. Data were fit with a Hill equation, with pKa = 7.23 and a slope of 1.3. Each point was calculated from a dataset with $n \geq 3$.

The deactivation kinetics of M314N channels were slower than WT at pH 7, and the G-V curves were left-shifted as compared with WT, in both 0 Ca^{2+} and 200 µM Ca^{2+} (Figs. 8 C, 1 and 2, and 9 C, 1 and 2). The G-V curves and deactivation kinetics at pH 9 were similar to those at pH 7, in either 0 Ca^{2+} or 200 µM Ca^{2+} (Figs. 8 C, 1 and 2, and 9 C, 1 and 2). pH 5 led to leftward shift of G-V curves in 0 Ca^{2+} and rightward shift of G-V curves in 200 µM Ca^{2+}, as compared with pH 7 (Fig. 8 C, 1 and 2). Comparing these observations to M314D, the asparagine (N)-substituted channels were no longer constitutively open, and the pH-dependent gating seen in M314D was absent from M314N. Acidic pH–induced G-V shifts in M314N followed the direction of those in WT channels, which should be through the RCK1 histidine mechanism.

Consistent with this interpretation, the positions of the G-V curves in the background of RCK1 substitution M314N:H365R:H394R mutant were all left-shifted when compared with (M314 (WT):H365R:H394R) under the same conditions (Fig. 8 D, 1 and 2, and Tables I and II). Deactivation was slower than WT under all tested conditions. But there was very little pH dependence in deactivation kinetics or G-V curves in either 0 Ca^{2+} or 200 µM Ca^{2+} (Fig. 9 D, 1 and 2). The small rightward shifts by pH 8 and pH 9 in 0 Ca^{2+} may reflect the fact that the substituted arginines (R) in the RCK1 domain could have been partially neutralized under these conditions, as seen for M314 (WT):H365R:H394R (Fig. 1 B, 1).

The difference between glutamate (E) and glutamine (Q) substitutions, as well as the difference between aspartate (D) and asparagine (N) substitutions, especially the lack of pH-dependent changes in gating behavior for the nonionizable analogue–substituted mutants, led us to believe that the ionizable side chains of the charged residues were essential for the position 314–mediated, pH-dependent gating effects.

The open-state charge stabilization hypothesis

Results from all the mutants were so far consistent with the central argument of both the closed-state charge interaction (Fig. 3 C, 1) and the open-state charge stabilization (Fig. 3 C, 2) hypotheses. That is, charges at the 314 position help activate BK channels. In addition, we consistently saw slowing of deactivation τ_{app} at extreme negative voltages, by order(s) of magnitude, with charges at 314, arguing in favor of the open-state hypothesis. The following observations also argued against the closed-state hypothesis and lent more support to the open-state hypothesis.

First of all, the proposed destabilization of the closed state by negative electrostatic interactions between the four 314 side chains in the pore should be greater when the charges are closer to each other. Therefore, for the shortest aspartic acid side chains to interact with each other and cause the most dramatic effect on channel gating, the cavity of the pore at this position needs to be

sufficiently small. But the fact that charged amino acids with longer side chains (glutamic acid and lysine) also led to significant gating effects is at odds with this prediction. In fact, the even larger arginine (R) was tolerated at this position (M314R), with a gating phenotype very similar to that of M314K (Fig. S2). It seems that the pore is quite large at this position to accommodate the large arginine side chains from the four subunits. But this presumed large distance between equivalent residues from different subunits would make it more difficult for the charges of the shorter side chains to interact.

Second, glutamate and aspartate have essentially the same pKa (~4.0) in water, yet the difference between M314E and M314D channels was obvious. The side chain of glutamate is longer than that of aspartate by only one alkyl group, which also makes it more hydrophobic. M314E deactivation in 0 Ca^{2+} was slowed at basic pH levels considerably above the pKa value for glutamate in water (~4) (Fig. 4), implying a nonpolar environment for glutamate when the channel is closed.

Ionic strength experiments to further differentiate between the two hypotheses

An essential difference between the two hypotheses is that the closed-state hypothesis heavily relies on the proposed charge interaction, whereas the open-state hypothesis does not. Because the most dramatic and consistent charge-dependent changes in gating behavior were in the deactivation kinetics, we tested whether the pH-sensitive changes in deactivation depended on charge interaction by manipulating ionic strength of the intracellular solution. Lower ionic strength, by reducing shielding, should promote charge–charge interactions; higher ionic strength, by increasing shielding, should weaken such interactions. Therefore, if the slower deactivation was a result of charge–charge interactions, reducing ionic strength should lead to greater slowing, whereas increasing ionic strength should lead to less slowing.

To manipulate ionic strength, we replaced various amounts of K^+ in the intracellular solution with sucrose (Brelidze and Magleby, 2005). We limited the conditions

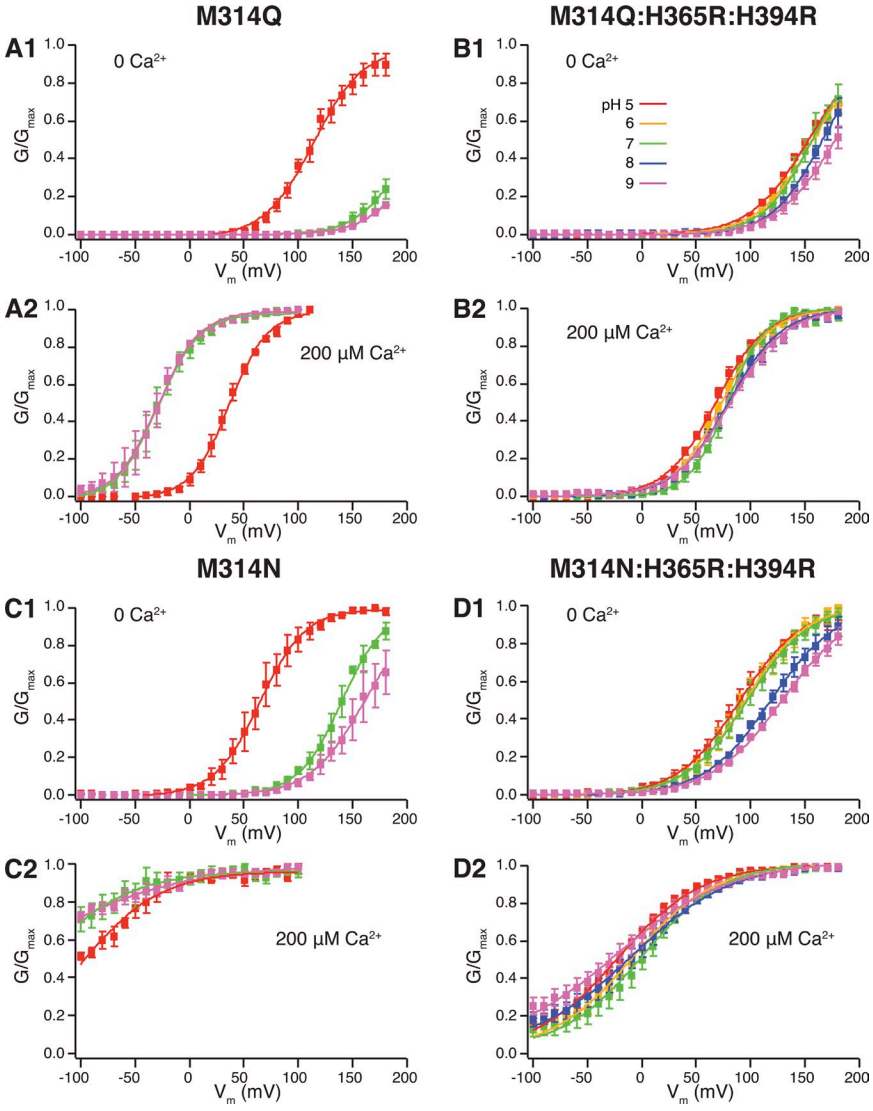

Figure 8. (A; 1) pH-dependent G-V shifts in M314Q BK channels in nominal 0 Ca^{2+}; (2) pH-dependent G-V shifts in M314Q BK channels in 200 µM Ca^{2+}; (B; 1) pH-dependent G-V shifts in M314Q:H365R:H394R channels in nominal 0 Ca^{2+}; (2) pH-dependent G-V shifts in M314Q:H365R:H394R channels in 200 µM Ca^{2+}; (C; 1) pH-dependent G-V shifts in M314N BK channels in nominal 0 Ca^{2+}; (2) pH-dependent G-V shifts in M314N BK channels in 200 µM Ca^{2+}; (D; 1) pH-dependent G-V shifts in M314N:H365R:H394R channels in nominal 0 Ca^{2+}; (2) pH-dependent G-V shifts in M314N:H365R:H394R channels in 200 µM Ca^{2+}. (See Tables I and II for fitting parameters.) Each point was calculated from a dataset with $n \geq 3$.

to 0 Ca^{2+}, pH 5 for M314H and 0 Ca^{2+} and pH 9 for M314E. Under these conditions, the deactivation kinetics were well within the dynamic range for further change, which would help reveal any potential changes introduced by adjustment of ionic strength.

As shown in Fig. 10, adjusting ionic strength by as much as 20-fold only slightly affected the deactivation τ_{app} for M314H across voltages from −190 to 0 mV (20.68 ± 3.24 ms and $n = 4$, at −190 mV in 14 mM K^+; 12.04 ± 2.26 ms and $n = 4$, in 284 mM K^+) (Fig. 10 A, 1, 2, and 3). In the case of M314E, high ionic strength in 284 mM K^+ resulted in a small but significant increase of deactivation τ_{app} as compared with lower K^+ concentrations (29.62 ± 5.10 ms and $n = 4$, at −190 mV in 14 mM K^+; 65.12 ± 7.18 ms and $n = 5$, in 284 mM K^+; P = 0.007) (Fig. 10 B, 1, 2, and 3). The direction of change was opposite to what one would predict from the closed-state charge interaction hypothesis (see above). It seems more likely that the X314 side-chain–exposed conformation corresponded to the open state of the BK channel. On one hand, it was energetically more favorable for the side-chain charges to stay in the pore-exposed positions and stabilize the open conformation. On the other hand, the pore-exposed charges from different subunits may repel each other and destabilize the open conformation. Reducing charge interaction by the higher ionic strength offset the destabilization forces and further exaggerated the stabilization effects, hence the even slower deactivation (Fig. 10 B, 3).

DISCUSSION

The understanding of ion channel–gating mechanisms has benefitted greatly from high-resolution structure models of some K^+ channels (Doyle et al., 1998; Jiang et al., 2002; Long et al., 2005). These structural models serve

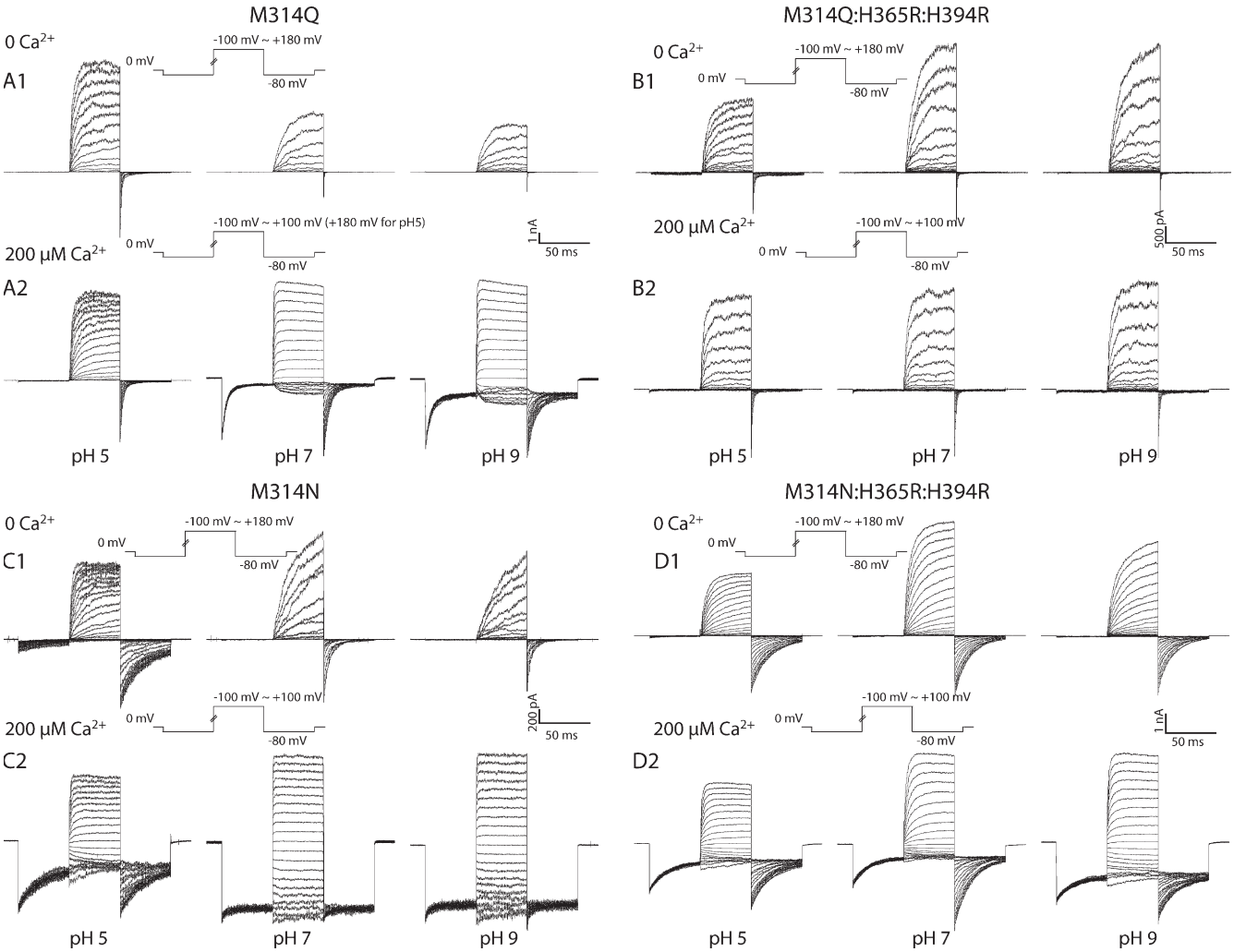

Figure 9. (A) Current traces in response to activation voltage protocols for M314Q channels in 0 Ca^{2+} (1) and 200 µM Ca^{2+} (2) in pH 5.0 (left), pH 7 (middle), and pH 9 (right). (B) Current traces in response to activation voltage protocols for M314Q:H365R:H394R channels in 0 Ca^{2+} (1) and 200 µM Ca^{2+} (2) in pH 5.0 (left), pH 7 (middle), and pH 9 (right). (C) Current traces in response to activation voltage protocols for M314N channels in 0 Ca^{2+} (1) and 200 µM Ca^{2+} (2) in pH 5.0 (left), pH 7 (middle), and pH 9 (right). (D) Current traces in response to activation voltage protocols for M314N:H365R:H394R channels in 0 Ca^{2+} (1) and 200 µM Ca^{2+} (2) in pH 5.0 (left), pH 7 (middle), and pH 9 (right).

as snapshots of the channel structure. Some of them depict probable open channels (Jiang et al., 2002; Long et al., 2005), whereas others depict probable closed ones (Doyle et al., 1998). In rare cases, some structural studies capture the channels in multiple states with a range of "openness" at different pore locations (Cuello et al., 2010a,b). Despite these advances, it remains difficult to obtain high-resolution structures of most K^+ channels, and the ones that are available, by themselves, tell little about the dynamics of gating conformational changes. Nevertheless, the known structures of related channels serve as guides and offer testable hypotheses for functional studies. Fundamental aspects of gating conformational change may be elucidated by a combination of structural information together with functional studies that can be interpreted within the structural framework. We have studied dynamics of the pore region of BK channels with the structural models of Kv1.2 and MthK channels as references.

We identified a deep-pore residue in the BK channel (M314 in hSlo1) as a marker for structural dynamics during channel gating. Our analysis was based on the energetic preference of charges toward polar environments. The same principle is behind aspartate scanning substitution studies to identify pore-facing residues in the transmembrane domains of the two-pore K^+ channels (Kollewe et al., 2009). With histidine substitution and adjustment of intracellular pH, the hydrolysis states of the histidine side chain have been modified to probe the pore structure of the nAChR channels (Cymes et al., 2005; Cymes and Grosman, 2008). We extended these methods to include more amino acid substitutions and a wider range of hydrolysis conditions.

With charge substitution at the M314 position, we found a new way to activate these mutant BK channels. That is, in addition to Ca^{2+}, depolarization, and H^+ binding to the RCK1 domain (Fig. 11 A), charging the X314 residues could also stabilize the open state of the mutant channels (Fig. 11 B). The charge stabilization effect at this pore-lining residue indicates an open conformation where the 314 side chains should have a larger degree of pore exposure than what is depicted in the Kv1.2-based BK structure, where the 314 residue is completely buried in the rest of the protein. Therefore, although the Kv1.2 model represents an open-state structure for the Kv1.2 channels, it did not seem to fit a BK open state, at least in some details. The MthK model, on the other hand, has the equivalent 314 position more exposed to the pore, but the resolution is not as good as the Kv1.2 model in this region. A more quantitative measurement of the state-dependent degree of pore exposure for the X314 side chains may be achieved by using probing molecules of various sizes and properties.

During the experiments with pH manipulations, we observed a proton "blocking" effect that was obvious in WT and all of the mutant channels (Figs. 2, 5, 6, and 9,

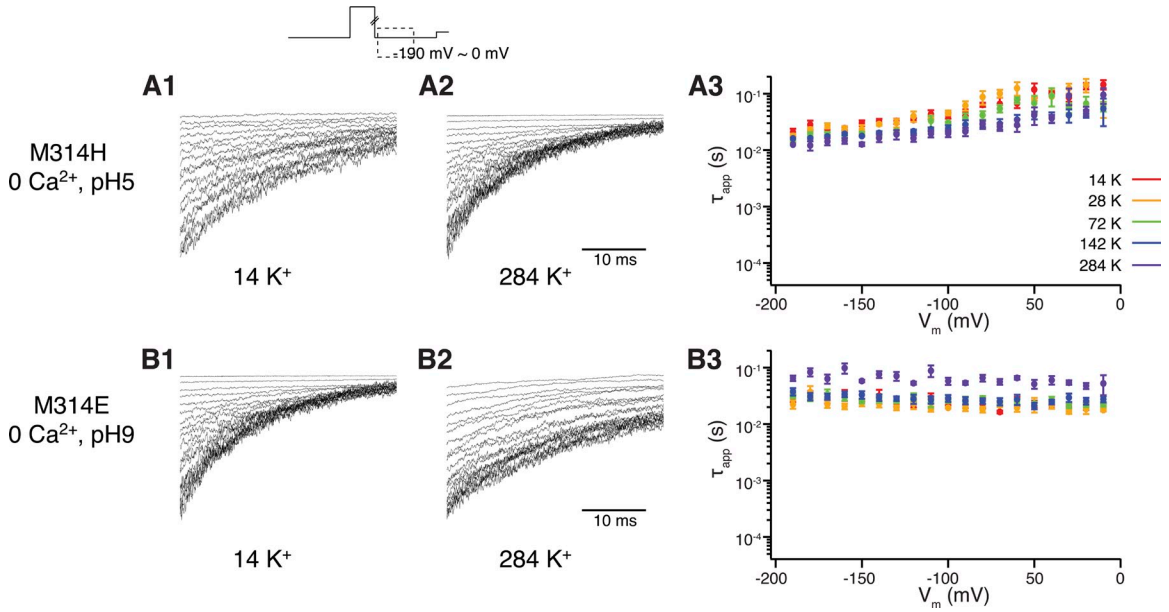

Figure 10. Current traces in response to deactivation voltage protocols. The patch was held at 0 mV, stepped to +100 mV to activate the channels, and then down to voltage levels of −190 to 0 mV to deactivate the channels, with 10-mV increments between sweeps. Current traces of the first 35 ms of the deactivation period are shown. (A; 1) Experiments were done for M314H, 0 Ca^{2+}, pH 5, in low ionic strength, with 14 mM K^+ in the intracellular solution. (2) Experiments were done for M314H, 0 Ca^{2+}, pH 5, in high ionic strength, with 284 mM K^+ in the intracellular solution. (3) τ_{app}–V relations of M314H in pH 5 and 0 Ca^{2+}, with various ionic strength. (B; 1) Experiments were done for M314E, 0 Ca^{2+}, pH 9, in low ionic strength, with 14 mM K^+ in the intracellular solution. (2) Experiments were done for M314E, 0 Ca^{2+}, pH 9, in high ionic strength, with 284 mM K^+ in the intracellular solution. (3) τ_{app}–V relations of M314E in pH 9 and 0 Ca^{2+}, with various ionic strength. Each point was calculated from a dataset with $n \geq 3$.

compare pH 5 traces to pH 7 and pH 9 in 200 µM Ca^{2+}). This is largely because of a reduction in apparent single-channel conductance and is probably a result of H^+ competing with K^+ for pore occupancy (Brelidze and Magleby, 2004). This "block" may explain why a G-V shift in low pH (pH 5) conditions was not obvious in previous studies (Hou et al., 2008). To obtain G-V curves for each condition, we normalized the tail currents to the maximum current amplitudes under the same pH conditions in saturating Ca^{2+}, in the same membrane patch. In few cases, even in Ca^{2+} concentrations as high as 200 µM and voltages as high as +200 mV, we could not achieve a maximum open probability (M314K:H365R:H394R, pH 8.0 and pH 9; Fig. 4 B, 2). For this particular case, maximum current levels in 200 µM Ca^{2+} and pH 7 were used to normalize the tail current amplitudes in pH 8 and pH 9, as in those cases, there was not much proton block between pH 7 and these two basic pH conditions (Fig. 5 C).

The difficulty in finding a saturating P_{open} value also led us to abandon the use of the H365A:H394A mutants to eliminate the RCK1-mediated H^+ activation mechanism (Hou et al., 2008). These alanine (A)-substituted mutants right-shifted the G-V curves as compared with WT and made it hard to obtain reliable G-V fitting within our experimental voltage ranges (up to +200 mV). Instead, we were successful in using the arginine (R)-substituted mutants (H365R:H394R) to eliminate the RCK1-mediated H^+ activation mechanism (Hou et al., 2008). The downside of the R-substituted mutants is that the R side chain is still ionizable, so that in basic pH (pH 8 and pH 9), in some mutants under certain conditions (for example, M314 (WT):H365R:H394R in 0 Ca^{2+}, M314K:H365R:H394R in both 0 and 200 µM Ca^{2+}, and M314N:H365R:H394R in 0 Ca^{2+}), there was a rightward shift of G-V curves as compared with pH 7. This can be explained by the basic pH partially neutralizing the R side chain. None of these shifts was in a direction that would confound our interpretation of the data. The ability of proton concentrations of pH 8 and pH 9 to affect the R side-chain charges implies a pKa value of these Rs that is lower than its pKa value in water (~12.5). Another observation worth noting for the R-substituted RCK1 mutants (X314:H365R:H394R) is that, although the G-V curves in 0 Ca^{2+} were left-shifted compared with their RCK1-WT counterparts, the G-V

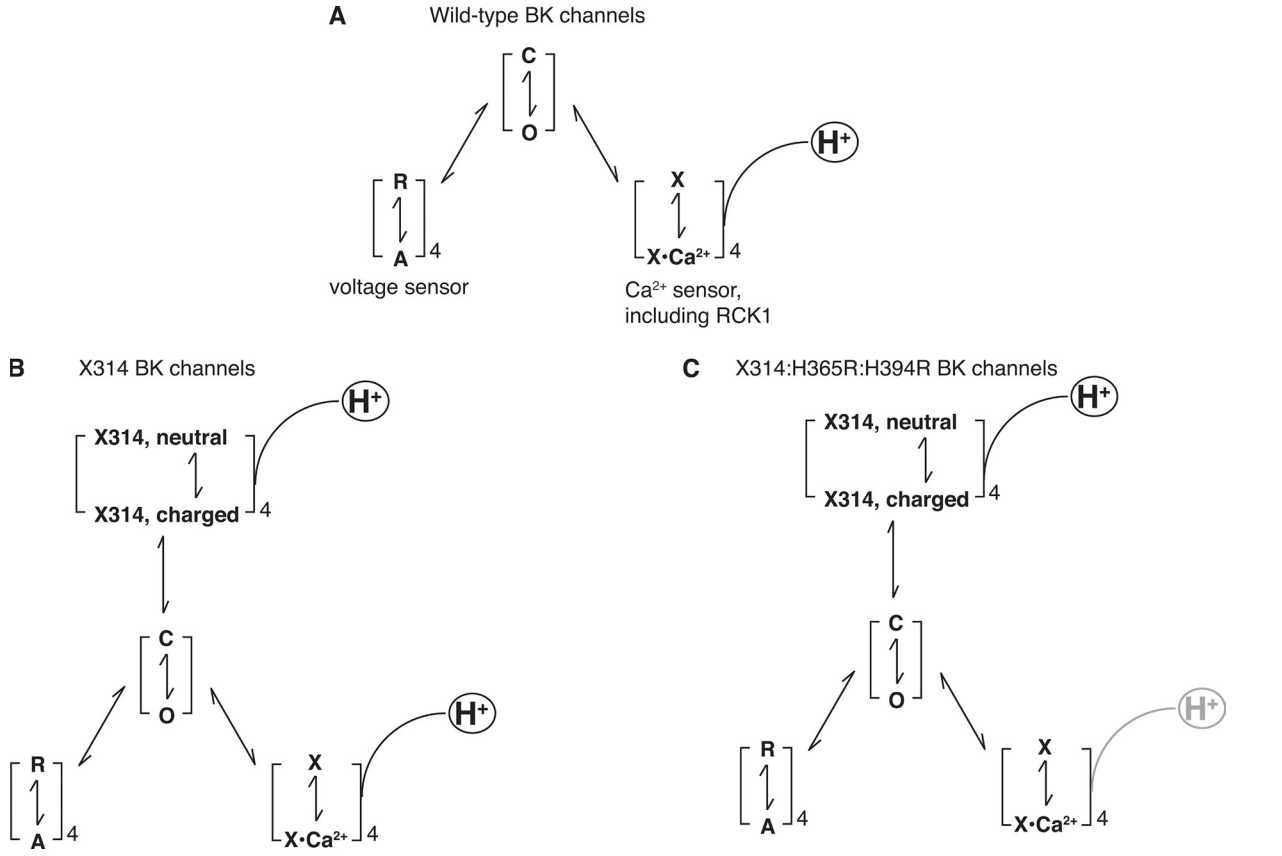

Figure 11. (A) Diagram of the BK channel-gating scheme. Both voltage (R↔A) and Ca^{2+} (X↔X·Ca^{2+}) can activate the channels (C→O). H^+ modulates the Ca^{2+}-binding transition (X↔X·Ca^{2+}) via the RCK1 domain. (B) With substitution into the 314 position by amino acids with ionizable side chains, charging the 314 side chains could bias the C↔O transition toward O (open). H^+ is also involved in this process (X314, neutral↔charged). (C) In X314:H365R:H394R channels, H^+ no longer affects the gating process via the RCK1-mediated mechanism.

curves in 200 μM Ca^{2+} were all right-shifted compared with their RCK1-WT counterparts, in neutral pH (pH 7). Therefore, these substitutions (H365R:H394R) seem to have led to a reduction in Ca^{2+} sensitivity of the BK channels. All of these results are consistent with recent structural data of the BK C terminus (Wu et al., 2010; Yuan et al., 2010), and with the idea that conformational changes in the RCK1 domain, via Ca^{2+} or H^+ binding, contribute to the Ca^{2+} activation pathway (Xia et al., 2002; Hou et al., 2008).

Even without the RCK1 domain mutants, using only the single X314 mutants, we were able to separate the X314-mediated mechanism from the RCK1-mediated mechanism of H^+ effects, by looking at deactivation kinetics in addition to G-V shifts. In all of the single mutants with ionizable side chains, the deactivation kinetics were consistently slower in conditions where the side chains were likely to be charged (acidic for H and K; basic for E and D) than in conditions where the side chains were likely to be neutral (basic for H and K; acidic for E and D), no matter which direction the G-V was shifted. For example, in M314E (Fig. 4) with 0 Ca^{2+}, compared with pH 7, both acidic and basic conditions shifted the G-V curves to the left. But the deactivation kinetics faithfully followed changes in pH in one direction. That is, the more basic the solution (so that more glutamates at 314 are charged), the slower the deactivation τ_{app}. We fitted the deactivation of the BK channels with a single-exponential τ_{app} for this level of analysis. The values of the τ_{app}s reflect predominately the slowest rate-limiting step of a multistate kinetic scheme. According to previous kinetic analysis of BK channel gating, the slowest step in BK channel activation/deactivation is likely to be the C↔O transition of the pore itself, which comes after voltage- and calcium-initiated activation, and accounts for >90% of the time-dependent kinetics (Cox et al., 1997; Cui et al., 1997; Horrigan and Aldrich, 1999, 2002; Horrigan et al., 1999). Because our X314 mutations are located in the pore just below the selectivity filter, we argue that these charge substitutions may have affected the balance of this O↔C transition in the pore, making it slower. The RCK1 locations, on the other hand, may be involved in earlier steps of Ca^{2+} binding. While causing shifts in the steady-state G-V by biasing the channels toward an open conformation, the RCK1 conformational changes may not be involved in the kinetically rate-limiting step, thus contributing to a smaller degree to the deactivation kinetics (Zeng et al., 2005). Therefore, although the deactivation kinetics truthfully reflected the amount of charges on the X314 side chains, the direction and extent of G-V shifts were determined by a combination of X314 and RCK1 histidines, in terms of their charge/neutral status.

Under certain conditions, one of the two mechanisms seems to dominate. For example, with M314D (Fig. 6) in 0 Ca^{2+} and neutral or basic pH, the charges on the substituted aspartates were able to keep the channels open by themselves, without the help of Ca^{2+} or depolarization, or H^+ binding to RCK1. In pH 5, the charge neutralization on the substituted aspartates again seems to have overcome the RCK1 mechanism, so that pH 5 no longer promoted channel opening as in WT and some other mutants. Instead, the acidic conditions helped the channel close, according to the predictions of the 314-mediated mechanism.

The ability of protonation/deprotonation to manipulate the charge states of the side chains was essential for the pH-dependent, 314-mediated gating effects on the charge-substituted mutants, because such ability was absent when nonionizable analogues of glutamate or aspartate were substituted in. It is worth noting, however, that the asparagine substitution (M314N) led to a slow deactivation and leftward G-V shift in pH 7 as compared with WT. Although not ionizable, the asparagine side chain is polar, for which a pore-exposed conformation may also be energetically favorable.

Aspartate (D), with the smallest and most hydrophilic side chain among all the charge-carrying amino acids, was the most effective in keeping the channels open when substituted into the 314 position. This and further observations led us to propose a model in which the 314 side chains are exposed to the pore in the open conformation. Because of its small size, the aspartate side chains could presumably stay in the large-sized pore to stabilize the open conformation, without feeling the repelling forces from each other that would have pushed these side chains to turn away from the pore. For the larger side-chain charges, although they also stabilize the open conformation by preferring to stay in the pore, the extent of such stabilization may be limited by mutual electrostatic repulsion, hence the observed, less dramatic gating phenotypes in larger side-chain charge substitutions.

We concluded that the BK pore structure in the open state should have the M314 side chain exposed to the pore. This was unexpected based on the Kv1.2 open-channel model, but not without precedent. For example, when KcsA was the only high-resolution K^+ channel structure available, functional measurements revealed discrepancies between Shaker channel behaviors and the KcsA-based model (del Camino et al., 2000). Such discrepancies also exist for CNG channels (Johnson and Zagotta, 2001). We argue that the 314 side chains undergo a change in the degree of pore exposure during gating, because the estimated pKa values for the substituted side chains were much closer to neutral than their pKa values in bulk water (Figs. 4 and 7). This indicates that either the pore environment differs from that of bulk solution or that the 314 side chains were not exposed to the pore all the time (Cymes and Grosman, 2011). The pKa values of the 314-mediated gating effects likely reflected the pKa values of the side chains in

a nonpolar environment, not water. Like any other mutagenesis-based approach, we cannot completely rule out the possibility that our mutations and manipulations introduced an open state that is different from the open state(s) of the WT channel. However, the great consistency among all the mutations argues strongly for its relevance to normal channel gating. Our results highlight the fact that channel gating is a dynamic process and that the structural dynamics during gating may be different between different channels.

Different channels also offer different opportunities in our quest for an understanding of the general principles of channel gating. For several channels, Shaker and CNG being the most successful examples, the cysteine scanning mutagenesis approach has proven to be fruitful in elucidating the amino acid organization of the pore and the dynamics of structural rearrangements during gating (Yellen et al., 1994; Liu et al., 1996, 1997; Holmgren et al., 1997, 1998; Flynn and Zagotta, 2001; Flynn et al., 2001; Johnson and Zagotta, 2001). For nAChR, the linear free energy analysis has yielded a tremendous amount of insight into the structural details of the arrangement of the pore and how nAChR channels gate (Grosman et al., 2000; Cymes et al., 2002), as did the proton-probing method (Cymes et al., 2005; Cymes and Grosman, 2008, 2011). For BK channels, because of a large number of endogenous cysteines, the cysteine scanning approach is problematic (Tang et al., 2001; Zhang and Horrigan, 2005; Zhou et al., 2010). As we found out in this study, BK channels, possibly because of their large pore size (Li and Aldrich, 2004, 2006; Brelidze and Magleby, 2005; Wilkens and Aldrich, 2006; Tang et al., 2009), are quite tolerant for large side-chain substitutions in the pore. We were able to use charge substitutions to probe conformational changes in the pore. Similar methods may have an application in studying other channels or proteins with polar/nonpolar interfaces.

The authors thank Drs. D. Brent Halling, Daniel Johnston, Weiyan Li, and Jiusheng Yan for helpful discussions and comments on the manuscript.

The University of Texas at Austin and the National Institutes of Health supported this study.

Kenton J. Swartz served as editor.

Submitted: 21 March 2011
Accepted: 21 June 2011

REFERENCES

Barrett, J.N., K.L. Magleby, and B.S. Pallotta. 1982. Properties of single calcium-activated potassium channels in cultured rat muscle. *J. Physiol.* 331:211–230.

Brelidze, T.I., and K.L. Magleby. 2004. Protons block BK channels by competitive inhibition with K^+ and contribute to the limits of unitary currents at high voltages. *J. Gen. Physiol.* 123:305–319. doi:10.1085/jgp.200308951

Brelidze, T.I., and K.L. Magleby. 2005. Probing the geometry of the inner vestibule of BK channels with sugars. *J. Gen. Physiol.* 126:105–121. doi:10.1085/jgp.200509286

Choi, K.L., R.W. Aldrich, and G. Yellen. 1991. Tetraethylammonium blockade distinguishes two inactivation mechanisms in voltage-activated K+ channels. *Proc. Natl. Acad. Sci. USA.* 88:5092–5095. doi:10.1073/pnas.88.12.5092

Contreras, J.E., and M. Holmgren. 2006. Access of quaternary ammonium blockers to the internal pore of cyclic nucleotide-gated channels: implications for the location of the gate. *J. Gen. Physiol.* 127:481–494. doi:10.1085/jgp.200509440

Contreras, J.E., D. Srikumar, and M. Holmgren. 2008. Gating at the selectivity filter in cyclic nucleotide-gated channels. *Proc. Natl. Acad. Sci. USA.* 105:3310–3314. doi:10.1073/pnas.0709809105

Cox, D.H., J. Cui, and R.W. Aldrich. 1997. Allosteric gating of a large conductance Ca-activated K^+ channel. *J. Gen. Physiol.* 110:257–281. doi:10.1085/jgp.110.3.257

Cuello, L.G., V. Jogini, D.M. Cortes, A.C. Pan, D.G. Gagnon, O. Dalmas, J.F. Cordero-Morales, S. Chakrapani, B. Roux, and E. Perozo. 2010a. Structural basis for the coupling between activation and inactivation gates in K(+) channels. *Nature.* 466:272–275. doi:10.1038/nature09136

Cuello, L.G., V. Jogini, D.M. Cortes, and E. Perozo. 2010b. Structural mechanism of C-type inactivation in K(+) channels. *Nature.* 466:203–208. doi:10.1038/nature09153

Cui, J., and R.W. Aldrich. 2000. Allosteric linkage between voltage and Ca(2+)-dependent activation of BK-type mslo1 K(+) channels. *Biochemistry.* 39:15612–15619. doi:10.1021/bi001509+

Cui, J., D.H. Cox, and R.W. Aldrich. 1997. Intrinsic voltage dependence and Ca^{2+} regulation of *mslo* large conductance Ca-activated K^+ channels. *J. Gen. Physiol.* 109:647–673. doi:10.1085/jgp.109.5.647

Cymes, G.D., and C. Grosman. 2008. Pore-opening mechanism of the nicotinic acetylcholine receptor evinced by proton transfer. *Nat. Struct. Mol. Biol.* 15:389–396. doi:10.1038/nsmb.1407

Cymes, G.D., and C. Grosman. 2011. Tunable pK(a) values and the basis of opposite charge selectivities in nicotinic-type receptors. *Nature.*

Cymes, G.D., C. Grosman, and A. Auerbach. 2002. Structure of the transition state of gating in the acetylcholine receptor channel pore: a phi-value analysis. *Biochemistry.* 41:5548–5555. doi:10.1021/bi011864f

Cymes, G.D., Y. Ni, and C. Grosman. 2005. Probing ion-channel pores one proton at a time. *Nature.* 438:975–980. doi:10.1038/nature04293

del Camino, D., and G. Yellen. 2001. Tight steric closure at the intracellular activation gate of a voltage-gated K(+) channel. *Neuron.* 32:649–656. doi:10.1016/S0896-6273(01)00487-1

del Camino, D., M. Holmgren, Y. Liu, and G. Yellen. 2000. Blocker protection in the pore of a voltage-gated K+ channel and its structural implications. *Nature.* 403:321–325. doi:10.1038/35002099

Doyle, D.A., J. Morais Cabral, R.A. Pfuetzner, A. Kuo, J.M. Gulbis, S.L. Cohen, B.T. Chait, and R. MacKinnon. 1998. The structure of the potassium channel: molecular basis of K+ conduction and selectivity. *Science.* 280:69–77. doi:10.1126/science.280.5360.69

Flynn, G.E., and W.N. Zagotta. 2001. Conformational changes in S6 coupled to the opening of cyclic nucleotide-gated channels. *Neuron.* 30:689–698. doi:10.1016/S0896-6273(01)00324-5

Flynn, G.E., J.P. Johnson Jr., and W.N. Zagotta. 2001. Cyclic nucleotide-gated channels: shedding light on the opening of a channel pore. *Nat. Rev. Neurosci.* 2:643–651. doi:10.1038/35090015

Grosman, C., M. Zhou, and A. Auerbach. 2000. Mapping the conformational wave of acetylcholine receptor channel gating. *Nature.* 403:773–776. doi:10.1038/35001586

Holmgren, M., P.L. Smith, and G. Yellen. 1997. Trapping of organic blockers by closing of voltage-dependent K^+ channels: evidence

for a trap door mechanism of activation gating. *J. Gen. Physiol.* 109:527–535. doi:10.1085/jgp.109.5.527

Holmgren, M., K.S. Shin, and G. Yellen. 1998. The activation gate of a voltage-gated K+ channel can be trapped in the open state by an intersubunit metal bridge. *Neuron.* 21:617–621. doi:10.1016/S0896-6273(00)80571-1

Horrigan, F.T., and R.W. Aldrich. 1999. Allosteric voltage gating of potassium channels II. Mslo channel gating charge movement in the absence of $Ca^{(2+)}$. *J. Gen. Physiol.* 114:305–336. doi:10.1085/jgp.114.2.305

Horrigan, F.T., and R.W. Aldrich. 2002. Coupling between voltage sensor activation, Ca^{2+} binding and channel opening in large conductance (BK) potassium channels. *J. Gen. Physiol.* 120:267–305. doi:10.1085/jgp.20028605

Horrigan, F.T., J. Cui, and R.W. Aldrich. 1999. Allosteric voltage gating of potassium channels I. Mslo ionic currents in the absence of $Ca^{(2+)}$. *J. Gen. Physiol.* 114:277–304. doi:10.1085/jgp.114.2.277

Hoshi, T., W.N. Zagotta, and R.W. Aldrich. 1991. Two types of inactivation in Shaker K+ channels: effects of alterations in the carboxy-terminal region. *Neuron.* 7:547–556. doi:10.1016/0896-6273(91)90367-9

Hou, S., R. Xu, S.H. Heinemann, and T. Hoshi. 2008. Reciprocal regulation of the Ca2+ and H+ sensitivity in the SLO1 BK channel conferred by the RCK1 domain. *Nat. Struct. Mol. Biol.* 15:403–410. doi:10.1038/nsmb.1398

Hou, S., F.T. Horrigan, R. Xu, S.H. Heinemann, and T. Hoshi. 2009. Comparative effects of H+ and Ca2+ on large-conductance Ca2+- and voltage-gated Slo1 K+ channels. *Channels (Austin).* 3:249–258.

Jiang, Y., A. Lee, J. Chen, M. Cadene, B.T. Chait, and R. MacKinnon. 2002. Crystal structure and mechanism of a calcium-gated potassium channel. *Nature.* 417:515–522. doi:10.1038/417515a

Johnson, J.P. Jr., and W.N. Zagotta. 2001. Rotational movement during cyclic nucleotide-gated channel opening. *Nature.* 412:917–921. doi:10.1038/35091089

Kollewe, A., A.Y. Lau, A. Sullivan, B. Roux, and S.A. Goldstein. 2009. A structural model for K2P potassium channels based on 23 pairs of interacting sites and continuum electrostatics. *J. Gen. Physiol.* 134:53–68. doi:10.1085/jgp.200910235

Li, W., and R.W. Aldrich. 2004. Unique inner pore properties of BK channels revealed by quaternary ammonium block. *J. Gen. Physiol.* 124:43–57. doi:10.1085/jgp.200409067

Li, W., and R.W. Aldrich. 2006. State-dependent block of BK channels by synthesized shaker ball peptides. *J. Gen. Physiol.* 128:423–441. doi:10.1085/jgp.200609521

Liu, Y., M.E. Jurman, and G. Yellen. 1996. Dynamic rearrangement of the outer mouth of a K+ channel during gating. *Neuron.* 16:859–867. doi:10.1016/S0896-6273(00)80106-3

Liu, Y., M. Holmgren, M.E. Jurman, and G. Yellen. 1997. Gated access to the pore of a voltage-dependent K+ channel. *Neuron.* 19:175–184. doi:10.1016/S0896-6273(00)80357-8

Long, S.B., E.B. Campbell, and R. Mackinnon. 2005. Crystal structure of a mammalian voltage-dependent Shaker family K+ channel. *Science.* 309:897–903. doi:10.1126/science.1116269

Marty, A., and E. Neher. 1985. Potassium channels in cultured bovine adrenal chromaffin cells. *J. Physiol.* 367:117–141.

Piskorowski, R.A., and R.W. Aldrich. 2006. Relationship between pore occupancy and gating in BK potassium channels. *J. Gen. Physiol.* 127:557–576. doi:10.1085/jgp.200509482

Rothberg, B.S., and K.L. Magleby. 2000. Voltage and Ca^{2+} activation of single large-conductance Ca^{2+}-activated K^+ channels described by a two-tiered allosteric gating mechanism. *J. Gen. Physiol.* 116:75–99. doi:10.1085/jgp.116.1.75

Tang, Q.Y., X.H. Zeng, and C.J. Lingle. 2009. Closed-channel block of BK potassium channels by bbTBA requires partial activation. *J. Gen. Physiol.* 134:409–436. doi:10.1085/jgp.200910251

Tang, X.D., H. Daggett, M. Hanner, M.L. Garcia, O.B. McManus, N. Brot, H. Weissbach, S.H. Heinemann, and T. Hoshi. 2001. Oxidative regulation of large conductance calcium-activated potassium channels. *J. Gen. Physiol.* 117:253–274. doi:10.1085/jgp.117.3.253

Wilkens, C.M., and R.W. Aldrich. 2006. State-independent block of BK channels by an intracellular quaternary ammonium. *J. Gen. Physiol.* 128:347–364. doi:10.1085/jgp.200609579

Wu, Y., Y. Yang, S. Ye, and Y. Jiang. 2010. Structure of the gating ring from the human large-conductance Ca(2+)-gated K(+) channel. *Nature.* 466:393–397. doi:10.1038/nature09252

Xia, X.M., X. Zeng, and C.J. Lingle. 2002. Multiple regulatory sites in large-conductance calcium-activated potassium channels. *Nature.* 418:880–884. doi:10.1038/nature00956

Yellen, G., D. Sodickson, T.Y. Chen, and M.E. Jurman. 1994. An engineered cysteine in the external mouth of a K+ channel allows inactivation to be modulated by metal binding. *Biophys. J.* 66:1068–1075. doi:10.1016/S0006-3495(94)80888-4

Yuan, P., M.D. Leonetti, A.R. Pico, Y. Hsiung, and R. MacKinnon. 2010. Structure of the human BK channel Ca2+-activation apparatus at 3.0 A resolution. *Science.* 329:182–186. doi:10.1126/science.1190414

Zeng, X.H., X.M. Xia, and C.J. Lingle. 2005. Divalent cation sensitivity of BK channel activation supports the existence of three distinct binding sites. *J. Gen. Physiol.* 125:273–286. doi:10.1085/jgp.200409239

Zhang, G., and F.T. Horrigan. 2005. Cysteine modification alters voltage- and $Ca^{(2+)}$-dependent gating of large conductance (BK) potassium channels. *J. Gen. Physiol.* 125:213–236. doi:10.1085/jgp.200409149

Zhou, Y., and R. MacKinnon. 2003. The occupancy of ions in the K+ selectivity filter: charge balance and coupling of ion binding to a protein conformational change underlie high conduction rates. *J. Mol. Biol.* 333:965–975. doi:10.1016/j.jmb.2003.09.022

Zhou, Y., X. Xia, and C.J. Lingle. 2010. Inhibition of large-conductance Ca2+-activated K+ channels by nanomolar concentrations of Ag+. *Mol. Pharmacol.* 78:952–960. doi:10.1124/mol.110.066407